Journal of Medicinal Chemistry

pubs.acs.org/jmc Article

Optimization of *N*-Phenylpropenoyl-L-amino Acids as Potent and Selective Inducible Nitric Oxide Synthase Inhibitors for Parkinson's Disease

Xiao-Long Hu, Xian-Yu Lv, Rong Wang, Huan Long, Jia-Hao Feng, Bao-Lin Wang, Wei Shen, Hao Liu, Fei Xiong,* Xiao-Qi Zhang, Wen-Cai Ye, and Hao Wang*

Cite This: *J. Med. Chem.* 2021, 64, 7760–7777 Read Online

ACCESS | Metrics & More | Article Recommendations | Supporting Information

ABSTRACT: *N*-Phenylpropenoyl-L-amino acids (NPAs) are inducible nitric oxide synthase (iNOS) inhibitors possessing preventive effects for Parkinson's disease (PD). Here, structural modifications for improving the iNOS inhibitory activity and blood–brain barrier (BBB) permeability of NPAs were conducted, leading to 20 optimized NPA derivatives (**1**–**20**). Compound **18**, with the most potent activity (IC_{50} = 74 nM), high BBB permeability (P_e = 19.1 × 10^{-6} cm/s), and high selectivity over other NOS isoforms, was selected as the lead compound. Further studies demonstrated that **18** directly binds to iNOS. In the 1-methyl-4-phenyl-1,2,3,6-tetrahydropyridine (MPTP)-induced acute PD model, the oral administration of **18** (1 and 2 mg/kg) exerted preventive effects by alleviating the loss of dopaminergic (DAergic) neurons. Notably, in the MPTP-/probenecid-induced chronic PD model, the same dose of **18** also displayed a therapeutic effect by repairing the damaged DAergic neurons. Finally, good pharmacokinetic properties and low toxicity made **18** a promising candidate for the treatment of PD.

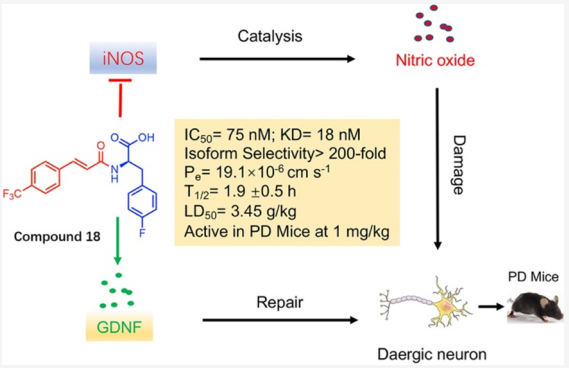

INTRODUCTION

Parkinson's disease (PD) is the second most common age-related neurodegenerative disorder characterized by the loss of dopaminergic (DAergic) neurons in the substantia nigra pars compacta (SNpc), which decreases the interstitial dopamine (DA) level, resulting in bradykinesia, rigidity, and tremor.[1] Current therapeutics mainly focus on the enhancement of the DA level, such as levodopa (L-DOPA), catechol-*O*-methyltransferase inhibitors, monoamine oxidase type B (MAO-B) inhibitors, and DA receptor agonists.[2−6] These available PD drugs offer valuable symptomatic relief but are often accompanied by serious side effects and cannot slow down the progression of PD.[7] Neuroinflammation is one of the hallmarks of PD and contributes to DAergic neuron degeneration.[8] Targeting excessive neuroinflammation could offer new therapeutic opportunities for PD and might slow down the disease progression.[8]

Inducible nitric oxide synthase (iNOS), the key enzyme for the synthesis process of toxic nitric oxide (NO), plays a critical role in inflammation and neuroinflammation.[9,10] NOS has three isoforms, including endothelial NOS (eNOS), neuronal NOS (nNOS), and iNOS, which are involved in the catalytic production of NO and maintaining normal physiological reactions.[11] Several studies have demonstrated that iNOS is overexpressed and overactivated in animals and patients with PD, indicating that iNOS is a key target for PD.[12−15] However, much work has been focused on iNOS inhibitors for acute inflammation, severe shock, and diabetes, and only a few are related to PD due to their poor efficiency, blood–brain barrier (BBB) permeability, and isoform selectivity.[16] Our previous efforts in achieving iNOS inhibitors with excellent potency have led to a class of molecules bearing a scaffold of *N*-phenylpropenoyl-L-amino acids (NPAs). Among these NPAs, hit compound **4b** (IC_{50} = 1.09 μM) has shown good efficacy for PD prevention in vitro and in vivo.[17] These results reported that NPAs are new potent iNOS inhibitors for PD therapy; therefore, further optimization of **4b** focusing on activity, isoform selectivity, and BBB permeability was necessary.

In this work, 20 additional optimized NPA derivatives (**1**–**20**), which possessed enhanced iNOS inhibitory effects and BBB permeability compared with those of **4b**, were designed and synthesized. Their structure–activity relationships (SARs) and structure–selectivity relationships were discussed. The preventive effects in the acute PD model and the therapeutic

Received: March 30, 2021
Published: May 21, 2021

https://doi.org/10.1021/acs.jmedchem.1c00578
J. Med. Chem. 2021, 64, 7760–7777

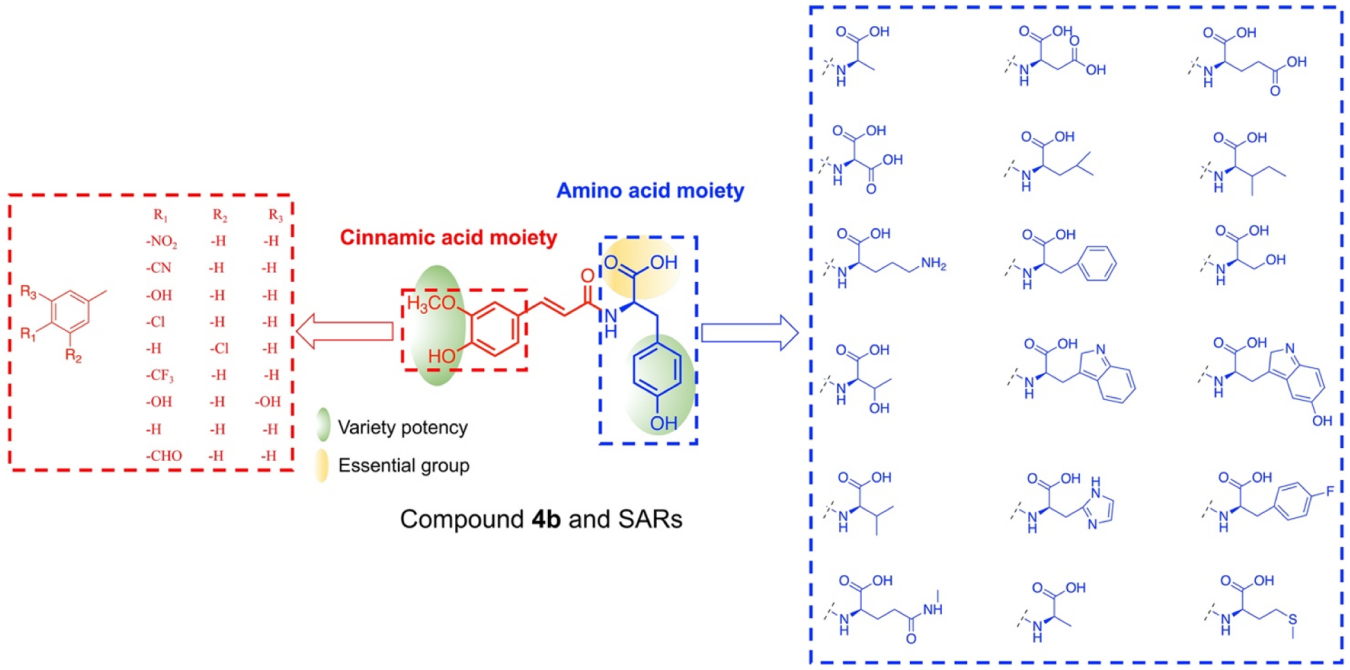

Figure 1. Strategies for further structural optimization of **4b**.

effects in the chronic PD model, the absorption, distribution, metabolism, excretion, and toxicity (ADME/Tox) profiles, and the pharmacokinetic profiles of the candidate compound were further investigated. This study led to the identification of highly potent compounds with significant improvement. Among them, compound **18** proved to be particularly promising.

RESULTS AND DISCUSSION

Design and Chemistry. Our previous study has demonstrated that NPAs, especially **4b** (Figure 1), are potent iNOS inhibitors with preventive effects in PD.[17] This hit compound matched "Lipinski's rule of five" and it also provided multiple diversification points for robust optimization. With careful analysis, it was supposed that the two phenolic hydroxy groups present in **4b** might bring some negative effects as follows: (1) the polar of the molecule is strong, which might affect the absorption and BBB permeability and (2) glucuronidation of multi-hydroxyl groups may shorten the action time of the compound within the body. Besides, **4b** was not potent enough and its activity should be improved in vitro and in vivo. Taken together, structural modifications were conducted to increase the iNOS inhibitory effect and BBB permeability of **4b**, as well as improve its physicochemical properties. According to the basic principles of drug design, the following strategies were used: (1) the structural skeleton, cinnamic acid moiety, and amino acid moiety (L-tyrosine) of **4b** were retained, and minimal modifications were made to the benzene ring of the cinnamic acid moiety to adjust the lipid−water partition coefficients and/or improve its stability/or improve its activity, such as changing the hydroxyl groups and introducing the nitrogen-containing groups, halogen, trifluoromethyl, or aldehyde groups (Figure 1) and (2) substantial changes were made to the amino acid moiety by replacing the L-tyrosine with several aliphatic amino acids, aromatic amino acids, and heterocyclic amino acids to enhance the pharmacological effects (Figure 1). Consequently, 209 compounds were designed belonging to the 19 series (**a**−**s**, Table S1). Then, molecular docking assay was used to predict the inhibitory effects of these 209 compounds on iNOS (PDB code: 1R35)[17,18] and ADME properties. The most important factor in identifying drugs for neurological diseases is their ability to penetrate BBB. In the Discovery studio software, only compounds with predicted BBB levels of 0, 1, or 2 were considered to permeate the BBB, while 3 or 4 were not. Usage of levels 0, 1, or 2 as the cutoff for ADMET_BBB_LEVEL ensured that only the compounds that could pass the BBB would be retained. In addition, the higher the absolute values of -CDOCKER energy are, the more stable the binding is. Notably, although some compounds, such as compounds **i-I**, **i-II**, and **i-III** and **j-I** and **s-I** (in Table S2), showed higher -CDOCKER energy than **4b**, their BBB levels were predicted to be level 3 or level 4 and therefore, they were not considered. As a result, 20 of these compounds (red font in Table S2) with the higher absolute values of -CDOCKER energy than **4b** (24.3 kcal/mol) and higher BBB permeability (level 1 or level 2) than **4b** (level 4) were screened out. Here, in this work, these 20 NPAs (**1**−**20**) were efficiently synthesized under mild and water-compatible conditions (Scheme 1). Notably, compounds **1**−**20** can be easily obtained in a 10 g scale without the use of column chromatography techniques.

Inhibitory Effects of 1−20 on NO Production and iNOS Activity. All the synthesized NPAs were tested for their anti-neuroinflammatory effects using a lipopolysaccharide (LPS)-induced BV-2 cell activation model. As shown in Figure 2, **1**−**20** exhibited stronger NO inhibitory effects than **4b**, especially **13**−**20** (1 μM, inhibition rate > 50%). The inhibitory effects of these compounds and **4b** on iNOS were further tested using the iNOS enzyme activity assay. Results showed that **13**−**20** also showed promising iNOS inhibitory effects with half maximal inhibitory concentration (IC_{50}) values ranging from 74 to 434 nM (Table 1), consistent with the tendency of NO inhibition. This result suggests that these

https://doi.org/10.1021/acs.jmedchem.1c00578
J. Med. Chem. 2021, 64, 7760−7777

Scheme 1. Synthesis of Compounds 1−20

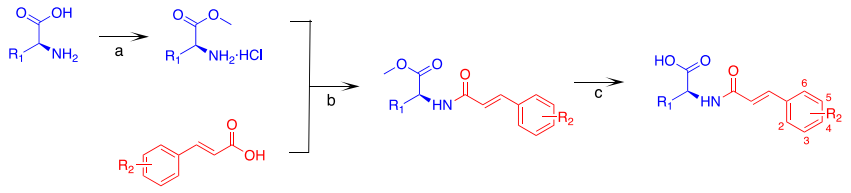

	R_1	R_2		R_1	R_2
1		2-Cl	**11**		3, 4-diCl
2	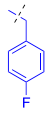	2-Cl	**12**		3, 4-diCl
3		2-Cl	**13**		4-F
4		2-Cl	**14**	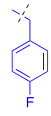	4-F
5		4-Cl	**15**		4-F
6	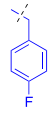	4-Cl	**16**		4-F
7		4-Cl	**17**		4-CF_3
8		4-Cl	**18**	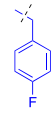	4-CF_3
9		3, 4-diCl	**19**		4-CF_3
10	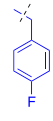	3, 4-diCl	**20**		4-CF_3

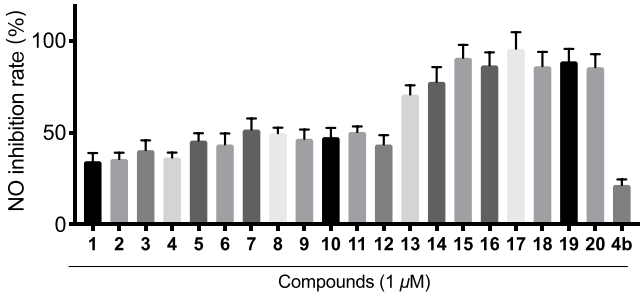

Figure 2. Effects of compounds **1**−**20** and **4b** on NO release in BV-2 cells.

compounds exerted anti-neuroinflammatory effects by targeting iNOS.

SAR Analysis and Three-Dimensional Quantitative Structure−Activity Relationship Model. SARs were discussed by structural moieties. For the cinnamic acid moiety, the C-4 position of the NPAs functionalized with one trifluoromethyl electron-withdrawing group (**17**−**20**, IC_{50} = 74−195 nM) can substantially increase iNOS inhibitory effects compared with that of the NPAs substituted by methyl (**13**−**16**, IC_{50} = 188−434 nM) and chlorine (**5**−**8**, IC_{50} = 731−945 nM) (Table 1), indicating that introducing an electronegative group to the C-4 position might increase the inhibitory effects of NPAs on iNOS. For the amino acid moiety, NPAs containing an aromatic amino acid moiety were found to exert stronger iNOS inhibitory effects than those with aliphatic amino acid moiety, such as the IC_{50} values of **13** (291 nM) and **14** (188 nM) < **15** (434 nM) and **16** (421 nM), respectively, as well as **17** (110 nM) and **18** (74 nM) < **19** (195 nM) and **20** (178 nM), respectively (Table 1). In addition, a three-dimensional quantitative SAR (3D-QSAR) model was built by Discovery Studio 3.0 (DS 3.0) software to evaluate the factors in correlation with in the bioassay results, and the structural features contributing to the corresponding activities. The results showed that the QSAR model was acceptable because the correlation coefficient (R^2) between the observed and predicted activities of training was 0.664, whereas that of the

https://doi.org/10.1021/acs.jmedchem.1c00578
J. Med. Chem. 2021, 64, 7760−7777

Table 1. Effects of 1−20 on NOS Activity and BBB Permeability

	IC_{50} (nM)			selectivity[a]		
comp.	iNOS	nNOS	eNOS	hnNOS/hiNOS	heNOS/hiNOS	Pe (10^{-6} cm s^{-1}) PAMPA-BBB
1	630 ± 38	64314 ± 5320	66194 ± 5480	102	105	
2	820 ± 53	125618 ± 7860	147301 ± 9870	153	180	
3	594 ± 41	20679 ± 1980	30605 ± 2400	51	52	
4	645 ± 33	25814 ± 2100	33142 ± 3100	35	51	
5	731 ± 67	102382 ± 9810	106370 ± 8920	140	146	
6	945 ± 84	156987 ± 10920	188770 ± 10020	166	199	
7	782 ± 56	39784 ± 3100	48850 ± 3950	51	62	
8	916 ± 88	56719 ± 4900	46610 ± 3980	62	51	
9	766 ± 65	110555 ± 9870	110680 ± 9810	151	144	
10	993 ± 67	148510 ± 9860	163860 ± 10210	149	165	
11	765 ± 74	29640 ± 2800	29745 ± 1800	39	39	
12	640 ± 34	25613 ± 2120	30560 ± 2000	40	48	
13	291 ± 25	31905 ± 2540	37620 ± 2980	110	129	4.61 ± 0.78
14	188 ± 13	34210 ± 2800	38000 ± 2700	182	202	4.32 ± 1.02
15	434 ± 29	18480 ± 1550	17100 ± 1250	43	39	4.88 ± 0.56
16	421 ± 41	20250 ± 1400	21050 ± 1590	48	50	4.97 ± 0.71
17	110 ± 7	11994 ± 980	15530 ± 1200	109	141	10.42 ± 0.97
18	74 ± 6	16650 ± 1010	18500 ± 1580	225	250	19.02 ± 1.32
19	195 ± 12	6120 ± 540	5600 ± 380	31	29	8.05 ± 1.00
20	178 ± 14	8360 ± 700	9600 ± 740	45	54	9.01 ± 0.89
4b	892 ± 45	40330 ± 2900	46590 ± 3800	47	52	1.23 ± 0.46
1400W[b]	8.4 ± 0.4	1980 ± 140	51200 ± 4520	236	6095	3.18 ± 0.95

[a]Selectivity = $IC_{50(\text{human nNOS})}/IC_{50(\text{human iNOS})}$; $IC_{50(\text{human eNOS})}/IC_{50(\text{human iNOS})}$. [b]1400W is a selective iNOS inhibitor, used as the reference control.

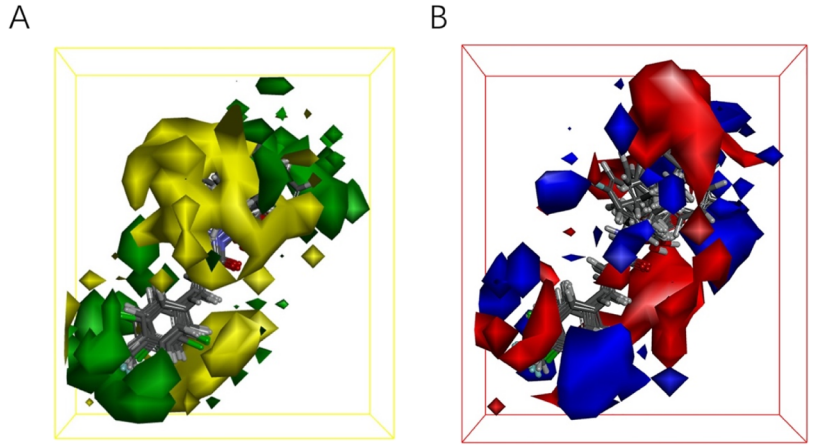

Figure 3. 3D-QSAR model. (A) 3D-QSAR model coefficients on electrostatic potential grids. Blue represents positive coefficients and red represents negative coefficients. (B) 3D-QSAR model coefficients on van der Waals grids. Green represents positive coefficients and yellow represents negative coefficients.

test set was 0.917 (Figure S1). The molecules aligned with the iso-surfaces of the 3D-QSAR model coefficients on van der Waals grids (Figure 3A) and electrostatic potential grids (Figure 3B) were also listed. Red contours in the electrostatic map indicate the regions where a high-electron density (negative charge) is expected to increase activity, and the blue contours represent regions where a low-electron density (partial positive charge) is expected to increase activity. Likewise, the steric map indicates the regions where steric bulk is predicted to increase (green) or decrease (yellow) activity. According to the maps, these compounds possessing a highly negative charge at the C-4 position and big bulk group would show higher iNOS inhibitory effects. These results provided a strategy for the design and optimization of NPA derivatives as potent iNOS inhibitors.

Isoform Selectivity. The current iNOS inhibitors have not been converted into clinically available drugs for PD due to their poor isoform selectivity for iNOS over eNOS and nNOS.[19] These two isoforms share very similar structural features in the active site as that of iNOS. The overinhibition of these two NOS isoforms should be avoided because they take part in the maintenance of normal physiological function.[16,19] First, eight compounds (**13**−**20**), with potent iNOS inhibitory effects, were selected for the evaluation of their NOS isoform selectivity. **13**, **14**, **17**, and **18** exhibited human eNOS/human iNOS selectivity, and human nNOS/human iNOS selectivity in the 100−250 range, especially **14** and **18** (in the range of 180−250). However, **15**, **16**, **19**, and **20** showed poor (<60-fold) isoform selectivity (Table 1). The results indicated that the NPAs containing an aromatic amino

https://doi.org/10.1021/acs.jmedchem.1c00578
J. Med. Chem. 2021, 64, 7760−7777

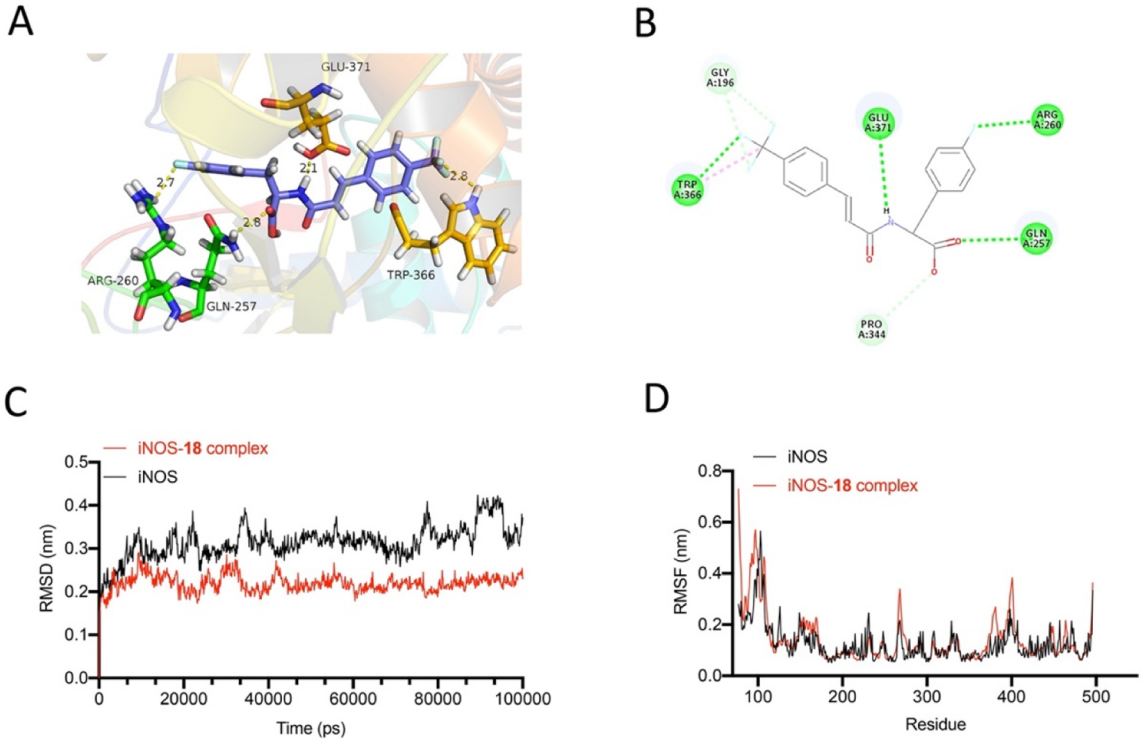

Figure 4. Molecular docking and MD simulation. (A) Predicted 3D binding mode of **18** with the iNOS crystal structure (PDB 1R35). Hydrogen bonds between inhibitors and amino acid residues are indicated by green dashed lines. (B) Predicted two-dimensional binding mode of **18** toward iNOS. (C) RMSD plot of native iNOS and complexed with EuC in black and red colors, respectively. (D) R_g plot of native iNOS and complexed with **18** in black and red colors, respectively.

acid moiety might have better iNOS selectivity than those with an aliphatic amino acid moiety. The NOS isoform selectivity of **1**−**12** was detected as corroborative evidence to further verify the inference. Table 1 shows that the NPAs with aromatic amino acid moieties (**1**, **2**, **5**, **6**, **9**, and **10**), respectively, show better iNOS selectivity than the NPAs with aliphatic amino acid moieties (**3**, **4**, **7**, **8**, **11**, and **12**). These results demonstrated that the aromatic amino acid moiety of NPAs contributed greatly to iNOS selectivity.

Effects of 13−20 on Artificial Membrane Permeability. The poor BBB permeability of reported iNOS inhibitors greatly limits the delivery of these compounds into the brain.[16] Therefore, **13**−**20** with potent inhibitory effects and selectivity were selected to evaluate their effects on cell membrane permeability through parallel artificial membrane permeability for the BBB (PAMPA-BBB) assay. In the PAMPA-BBB assay, a compound with good BBB penetration is classified as a central neural system (CNS) (+) molecule, if its effective permeability (P_e) is greater than 4.0×10^{-6} cm/s.[20] Results showed that **13**−**20** exhibited CNS (+) characteristics, and **17**−**20** (P_e = 8.05×10^{-6} to 19.02×10^{-6} cm/s) displayed higher permeability than **13**−**16** (P_e = 4.32×10^{-6} to 4.97×10^{-6} cm/s; Table 1). The results suggest that introducing trifluoromethyl functionality could improve the BBB permeability of NPAs (**17**−**20**) considerably. Replacing methyl (**13**) with the trifluoromethyl group (**17**) resulted in an approximately 2.5-fold increase in permeability and introducing fluorine on the aromatic ring of amino acids (**18**) resulted in an approximately 4.5-fold increase in permeability (Table 1). Therefore, introducing fluorine atoms into NPAs can increase the activity, selectivity, and BBB permeability of NPAs. Compound **18**, which had the most potent iNOS inhibitory effects, high isoform selectivity, and desirable BBB permeability, was selected as the lead compound for further exploration.

Docking and Molecular Dynamics Simulation of 18 Bound to iNOS. We used docking and atomistic force field-based molecular dynamic (MD) simulations to model **18** bound to iNOS. First, the crystal structure of iNOS (PDB code 1R35)[18] was used for the docking studies. As seen in Figure 4A,B, the protein aids ligand's anchoring within the pocket by the H bond between **18** and GLU371 (2.1 Å), TRP366 (2.8 Å), GLN257 (2.8 Å), and ARG260 (2.7 Å). The binding of a small molecule in the binding pocket of a protein can led to large conformational changes. Root-mean square deviation (RMSD) is one of the most important fundamental properties used to evaluate the structural stability of a protein.[21] Results showed that the average RMSD values of the iNOS and iNOS-**18** complexes were 0.31 and 0.21 nm, respectively (Figure 4C). The binding of **18** led to lower RMSD values at several parts and showed equilibration throughout the 100 ns MD simulations (Figure 4C). In addition, the average fluctuations of all residues and the root-mean square fluctuations (RMSFs) of iNOS upon ligand binding were plotted during the simulation as a function of the residue number to further assess local structural flexibility (Figure 4D). The RMSF plot reveals the residual fluctuations in iNOS at several regions of the protein structure. These residual fluctuations were minimized upon the binding of **18** throughout the simulations in a region spanning from the N-terminal to the C-terminal. These results suggested the strong binding between iNOS and **18**. Therefore, **18** might directly target iNOS.

18 Directly Binds to iNOS. Thermodynamic and kinetic experiments were carried out to evaluate the binding character

https://doi.org/10.1021/acs.jmedchem.1c00578
J. Med. Chem. 2021, 64, 7760−7777

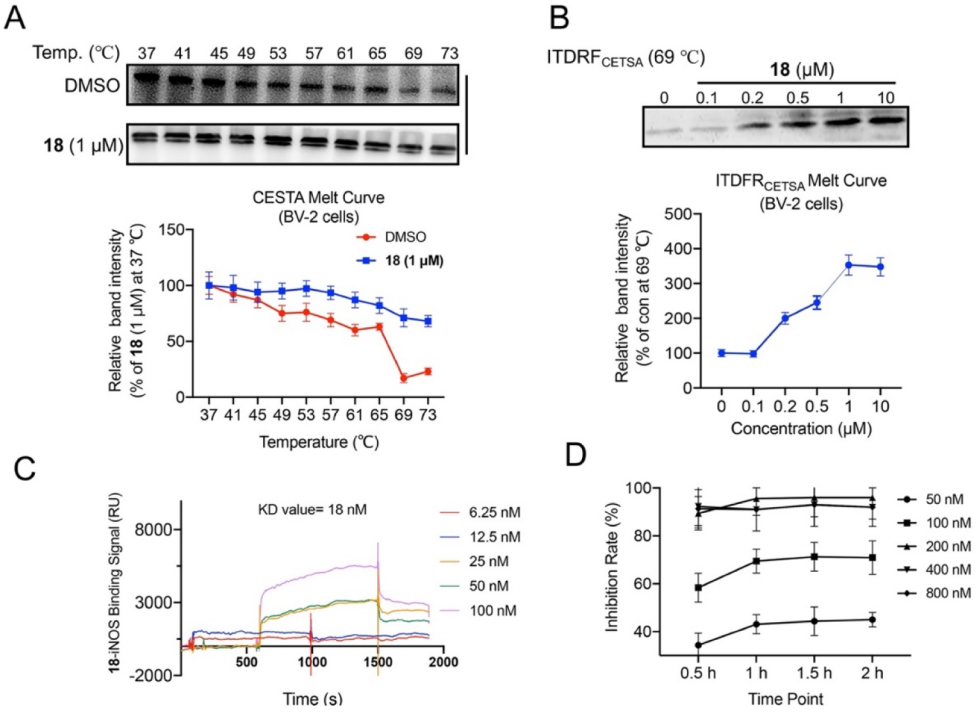

Figure 5. Thermodynamic and kinetic experiments of **18** toward iNOS. (A,B) CETSA and ITDRF$_{cesta}$ were used to evaluate the binding between **18** and iNOS at the thermodynamic level. (C) SPR was used to assess the binding between **18** and iNOS at the kinetic level. (D) Effects of **18** on iNOS activity at different time points (n = 3).

between **18** and iNOS. The cellular thermal shift assay (CETSA) was used in the thermodynamic test to study the thermal stabilization of the proteins upon ligand binding.[22,23] This assay has been used extensively on purified proteins to detect the interactions between donors and ligands. Results showed that the apparent aggregation temperatures were obtained with either **18** or dimethyl sulfoxide (DMSO), which could be compared, and substantial shifts demonstrated the binding of **18** and target proteins. Figure 5A shows that the thermal stabilization of iNOS increased compared with that of the control group (DMSO) after **18** was bound to iNOS. This thermal stabilization between **18** and iNOS was dose dependent according to the isothermal dose−response fingerprint (ITDRF) in CETSA (Figure 5B). Surface plasmon resonance, which is the most recognized method for studying the dynamic properties between ligands and donors,[24,25] was used in the kinetic test to further confirm the binding between **18** and iNOS. Results showed a strong binding between **18** and iNOS (K_D = 18 nM, Figure 5C). These results fully demonstrated that **18** directly binds to iNOS. In addition, **18** contained a Michael-acceptor moiety (propenamide), which is a common warhead of a number of drugs that irreversibly inactivate their targets. Therefore, a time-dependent inhibition study of treatment with iNOS was carried out to distinguish **18** between inhibitors and inactivators. Figure 5D shows that **18** had no time-dependent effects, suggesting **18** is an iNOS inhibitor rather than an inactivator.

18-Protected SH-SY5Y Cells from Neurotoxicity Induced by Microglial Activation. Microglia, a brain-resident immune cell, plays a central role in the process of PD by neuroinflammation. Activated microglia promote the production and activation of iNOS to generate overload NO, which make DAergic neurons more vulnerable to degeneration or toxicity.[26] In this study, the cell medium (CM) of BV-2 microglia treated with LPS was collected to stimulate DAergic neurons (SH-SY5Y cells), which were used to evaluate the in vitro anti-PD effects of **18**. Results showed that the cell viability of SH-SY5Y was decreased by 40% after 24 h of incubation with CM. However, CM derived from BV-2 cells with **18** (0.1, 1, and 10 μM) treatment for 6 h prior to LPS administration reduced SH-SY5Y cell injury in a dose-dependent manner (Figure 6A,B). Microscopic observation (Figure 6C), Hoechst 33258 staining (Figure 6D), and annexin V/FITC−propidium iodide (PI) double staining (Figure 6E,F) showed that **18** can reduce cell apoptosis in a dose-dependent manner. These results demonstrated that **18** can alleviate the injury of DAergic neurons induced by neuroinflammatory toxicity.

Pre-treatment of 18 Alleviated the PD-like Behavior of the 1-Methyl-4-phenyl-1,2,3,6-tetrahydropyridine-Induced Acute PD Model. 1-Methyl-4-phenyl-1,2,3,6-tetrahydropyridine (MPTP) produces a L-DOPA-responsive Parkinsonian syndrome, which is characterized by all the cardinal symptoms of PD and represents the best PD-like clinical picture obtainable in experimental animals.[27] In this study, traction test, rotarod test, and open-field test were used to evaluate the in vivo anti-PD effects of **18** in the MPTP-induced acute PD model (Figure 7A). The traction test showed that MPTP treatment decreased strength as the hind limb grip score of the MPTP model was lower than that of the control group. However, oral pre-treatment with **18** (1 or 2 mg/kg) can considerably increase the traction score. Therefore, prophylactic treatment with **18** could alleviate the reduction in the strength and equilibrium of muscles caused by MPTP (Figure 7B). The rotarod test showed that the time taken by MPTP-treated mice in the rotarod apparatus was remarkably reduced compared with the control. MPTP-treated mice that were given **18** stayed on the apparatus significantly

https://doi.org/10.1021/acs.jmedchem.1c00578
J. Med. Chem. 2021, 64, 7760−7777

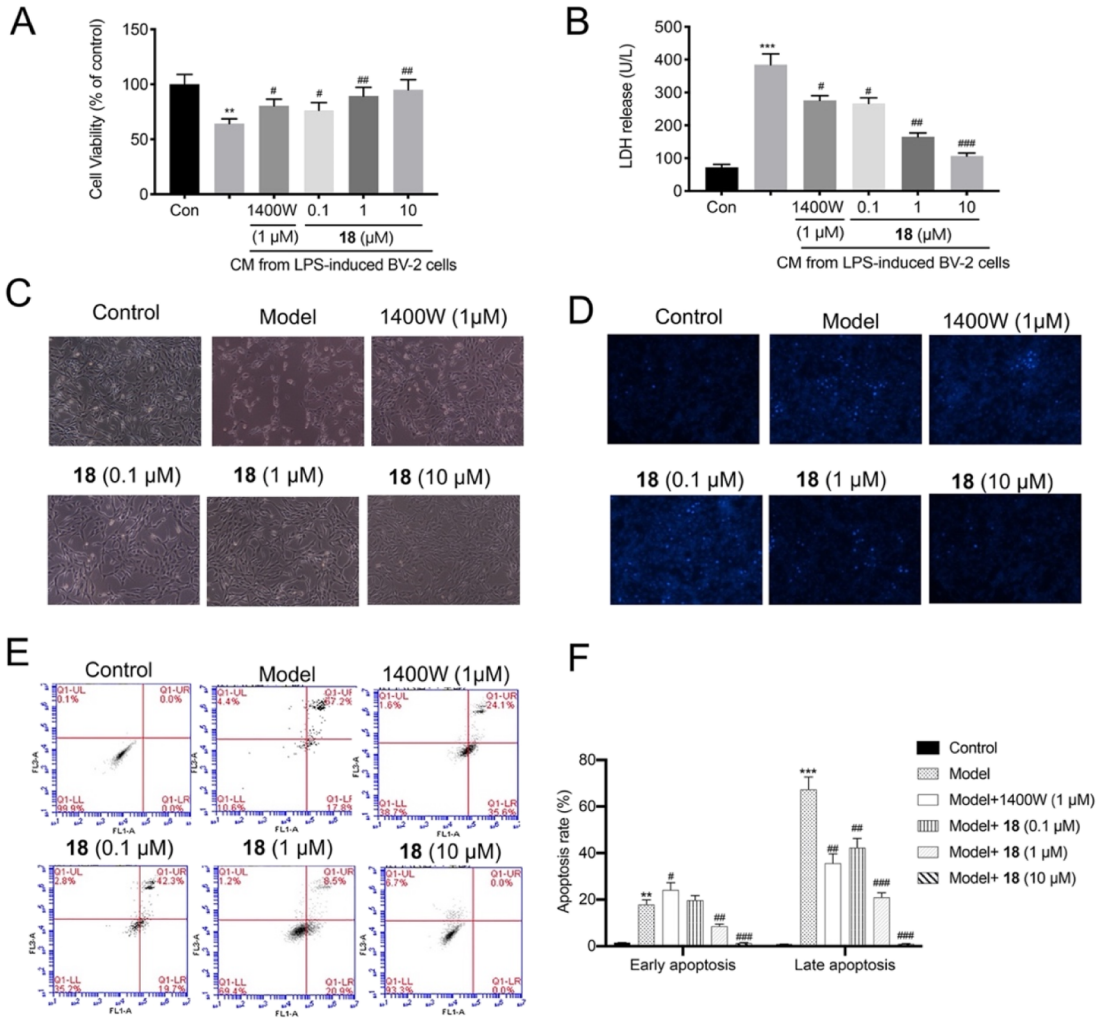

Figure 6. **18** protected DAergic neurons from neurotoxicity induced by microglial activation. SH-SY5Y cells were incubated for 24 h with conditioned medium derived from cultures of BV-2 cells. Before collecting culture media, BV-2 cells were pre-treated with **18** (0.1, 1, or 10 μM) for 2 h and incubated with LPS (0 or 500 ng/mL). (A) Cell viability measured with the MTT assay (n = 6). (B) LDH leakage assay (n = 6). (C) Morphological observation. (D) Cell nuclei stained with Hoechst 33258 (blue). (E) Apoptosis of SH-SY5Y cells evaluated by FCM detection of annexin V−PI double staining [distribution of viable (lower left), necrotic (upper left), late apoptotic (upper right), and early apoptotic (lower right) cells]. (F) Statistical analysis of three independent experiments of annexin V−PI double staining. All data are presented as means ± SD or SEM. $^{**}p < 0.01$ or $^{***}p < 0.001$, compared with the control group; $\#p < 0.05$, $\#\#p < 0.01$, or $\#\#\#p < 0.001$, compared with the LPS group.

longer than MPTP mice (Figure 7C). The open-field test showed that the total distances (Figure 7D,F) and average speed (Figure 7E) of the control and of the MPTP model group were substantially decreased and shortened, respectively, and the difference was statistically significant compared with those of the control group. The total distance and average speed of the MPTP + **18** group were significantly higher and longer compared with those of the model group. Although the positive drug, L-DOPA, showed similar effects, its dose−effect relationship was far less than that of **18**. These behavioral results suggested that **18** could effectively alleviate movement disorders related to acute PD and had a preventive effect on PD at low dosages.

Pre-treatment with 18 Decreased the Level of NO and Increased the Levels of DA and Tyrosine Hydroxylase in the MPTP-Induced Acute PD Model. MPTP remarkably induces DAergic neuron loss by activating the iNOS/NO/pathway in microglia cells, which results in the reduction of DA levels.[28] Results showed that MPTP remarkably increased the NO level and decreased the DA level in the SNpc and striatum (STR) compared with the control group. However, pre-treatment with **18** remarkably decreased the NO level and increased the DA level in the SNpc and STR compared with the MPTP group (Figure 8A,B). Tyrosine hydroxylase (TH), the rate-limiting step in the biosynthesis of DA, is commonly regarded as a marker of DAergic neurons to evaluate the degrees of PD. Results from the immunohistochemistry and immunoblotting of the TH protein showed that the number of TH positive cells (Figure 8C,D) and the expression of TH (Figure 8E) in the SNpc and STR of the MPTP-treated mice were decreased markedly compared with the control mice but were increased remarkably in the **18** pre-treated mice. These results indicated that **18** elicited neuroprotective effects against DAergic neuronal cell death in PD.

Pre-treatment of 18 Inhibited the Mitochondrial Apoptotic Pathway of SNpc and STR in the MPTP-Induced Acute PD Model. The apoptosis of DAergic neurons in the SNpc was the main reason for DA loss.[1] The mitochondria of DAergic neurons are a preferential target of

https://doi.org/10.1021/acs.jmedchem.1c00578
J. Med. Chem. 2021, 64, 7760−7777

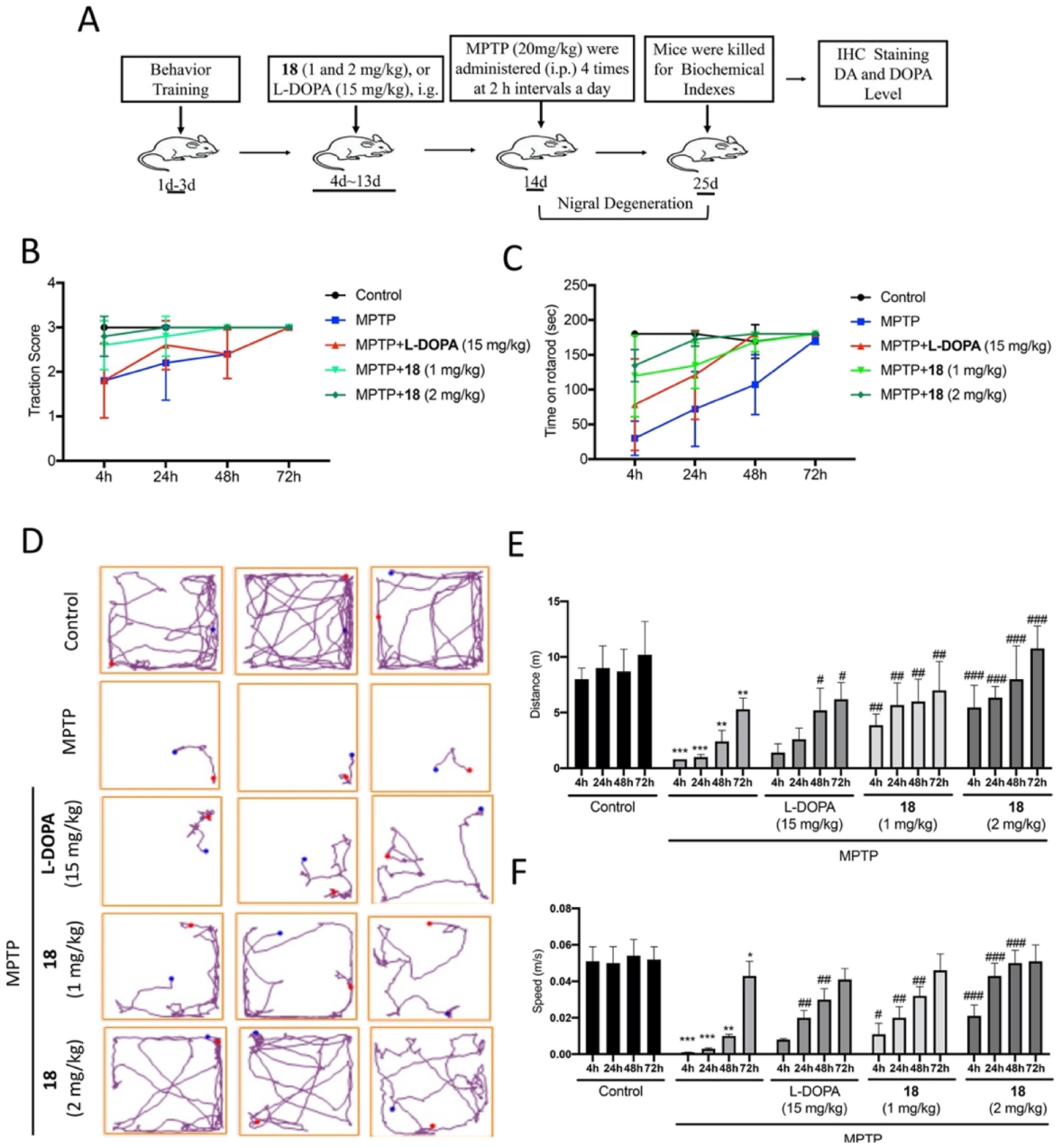

Figure 7. Prevention of **18** on MPTP-induced acute PD motor deficits. The behavioral measurements were carried out in the 4th, 24th, 48th, and 72nd h after the last injection of MPTP. (A) Experimental procedure and drug administration scheme. (B) Traction test. (C) Rotarod test. (D) Motion trail of the first three mice in each group in the open-field test (n = 8 mice/group). (E) Total distance of mice in the open-field test (n = 8 mice). (F) Mean velocity of mice in the open-field test (n = 8 mice). All data are presented as means ± SD. $^{**}p < 0.01$ or $^{***}p < 0.001$, compared with the control group; $\#p < 0.05$, $\#\#p < 0.01$, or $\#\#\#p < 0.001$, compared with the MPTP treatment group.

the NO induced by MPTP; thus, myriads of studies explored mitochondrial function in PD in the subsequent decades, and MPTP induction provides a formidable animal model of PD. Our results showed that the Bcl-2/Bax ratios in the SNpc and STR were remarkably decreased and the activities of caspase-3/9 in the SNpc and STR were increased in the MPTP-treated group compared with the control group. However, the pre-treatment with **18** can increase the Bcl-2/Bax ratio (Figure 9A) and decrease the activities of caspase-3 (Figure 9B) and caspase-9 (Figure 9B) in the SNpc (Figure 9C) and the STR (Figure 9D−F) in a dose-dependent manner. L-DOPA almost showed no inhibitory effects on mitochondrial apoptosis-related proteins. These results demonstrated that **18** can decrease the DAergic neuron loss by inhibiting the mitochondrial apoptotic pathway.

18 Showed a Therapeutic Effect in the MPTP/Probenecid-Induced Behavior Disorder of the Chronic PD Model. Most reported anti-PD agents were pre-treated to mice; hence, the agents possess preventive effects on PD but not therapeutic effects and have limitations in clinical application. Indeed, the DAergic nigrostriatal deficits obtained with the acute administration of MPTP (four injections over 1 day) tend to be reversible. The addition of probenecid potentiates the effects of MPTP, which allows the gradual loss of SNpc neurons and is associated with a substantial loss of striatal DA and DA uptakes.[29] This effect lasts for at least 6

https://doi.org/10.1021/acs.jmedchem.1c00578
J. Med. Chem. 2021, 64, 7760−7777

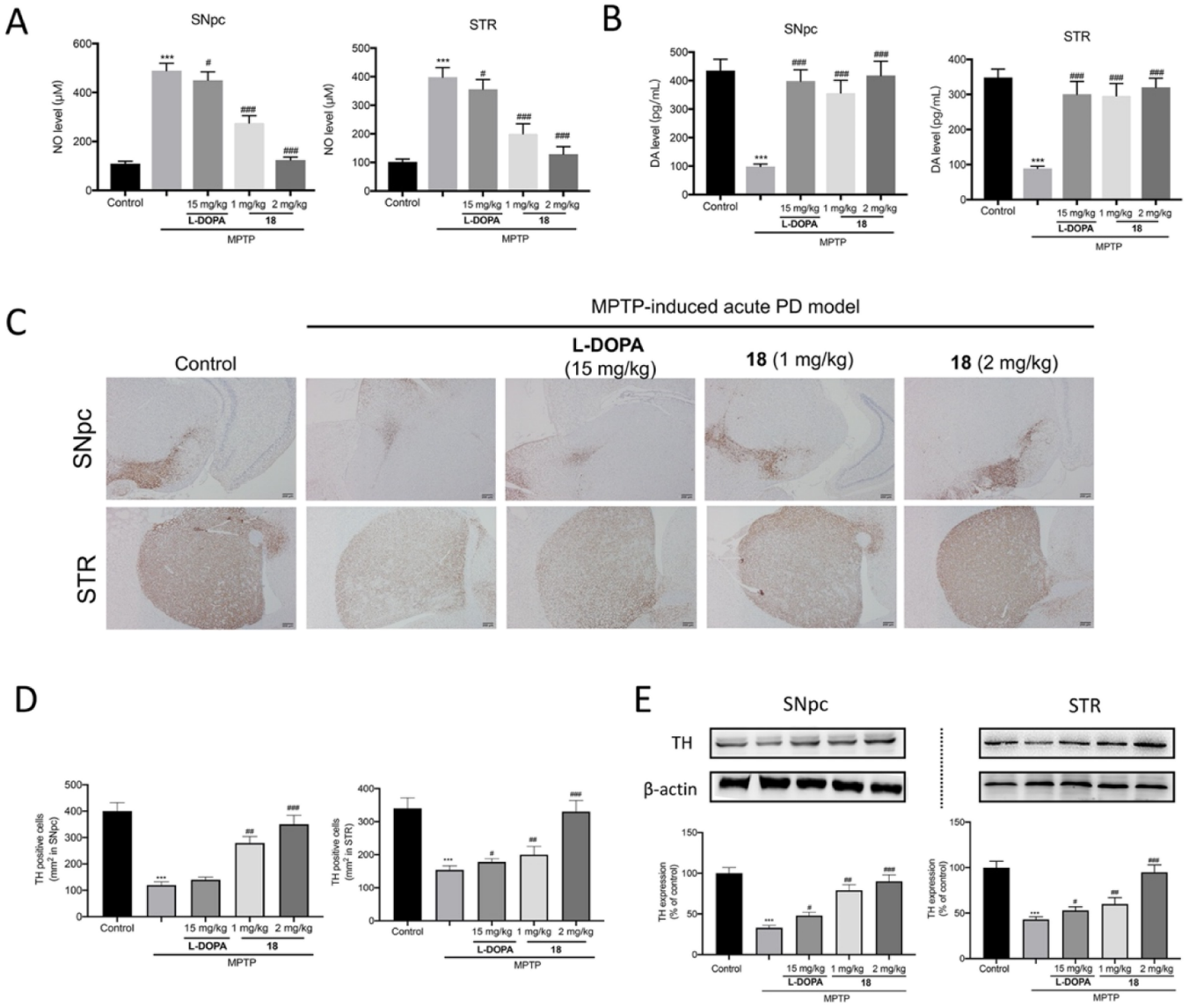

Figure 8. Prevention of **18** on MPTP-induced nigrostriatal DAergic injury. (A) Level of NO in SNpc and STR. (B) Level of DA in SNpc and STR. (C) Immunohistochemical staining showing TH positive cells in the SNpc and STR (scale bar: 200 μm). (D) Stereological counting of TH positive cells ($n = 6$). (E) Western blot analysis of the changes in the protein level of TH in both SNpc and STR. All data are presented as means ± SEM. $^{**}p < 0.01$ or $^{***}p < 0.001$, compared with the control group; $\#p < 0.05$, $\#\#p < 0.01$, or $\#\#\#p < 0.001$, compared with MPTP treatment group.

months after withdrawal from treatment. Therefore, in this section, the chronic MPTP/probenecid-induced mice model of PD (Figure 10A), which closely mimics the chronic and progressive neurodegeneration and behavioral deficits observed in human PD, was used to further investigate the therapeutic effect of **18** on PD.[29] Results showed that the mice began to have motor disorders in several behavior tests, namely, traction test (Figure 10B), pole test (Figure 10C), and open-field test (Figure 10D−G), after 30 days of MPTP/probenecid injection. However, oral treatment with **18** (1 or 2 mg/kg) considerably reversed these disorders, whereas L-DOPA did not. These behavior tests indicated that **18** had therapeutic effects on PD.

18 Can Increase the DAergic Neuron Loss Induced by MPTP/Probenecid. Behavior tests demonstrated that **18** can prevent and treat PD in very low dosages. The therapeutic effects suggest that **18** might have a function in the repairing of DAergic neuron injury in PD. Immunohistochemistry with TH and DOPA decarboxylase, the two key neural markers of DAergic neurons, was conducted to evaluate the repairing effect of **18** on DAergic neuron injury and verify the assumption. Results showed that the number of cells positive for TH and DOPA decarboxylase was remarkably decreased compared with the control group after 30 days of MPTP/probenecid injection. This result indicates that many DAergic neurons in the SNpc were lost. However, the number of TH- and DOPA decarboxylase positive cells increased after 20 consecutive days of treatment with **18** (Figure 11A−C). Western blot analysis showed that **18** can greatly increase the expression of TH and DOPA decarboxylase compared with the MPTP/probenecid group (Figure 11D,E). These results indicated that **18** can repair damaged DAergic neurons in PD.

Glial cell line-derived neurotrophic factor (GDNF), which is secreted by microglia, can promote the regeneration of DAergic neurons in the SNpc.[30,31] Therefore, the effect of **18** on GDNF secretion in glial cells was detected by

https://doi.org/10.1021/acs.jmedchem.1c00578
J. Med. Chem. 2021, 64, 7760−7777

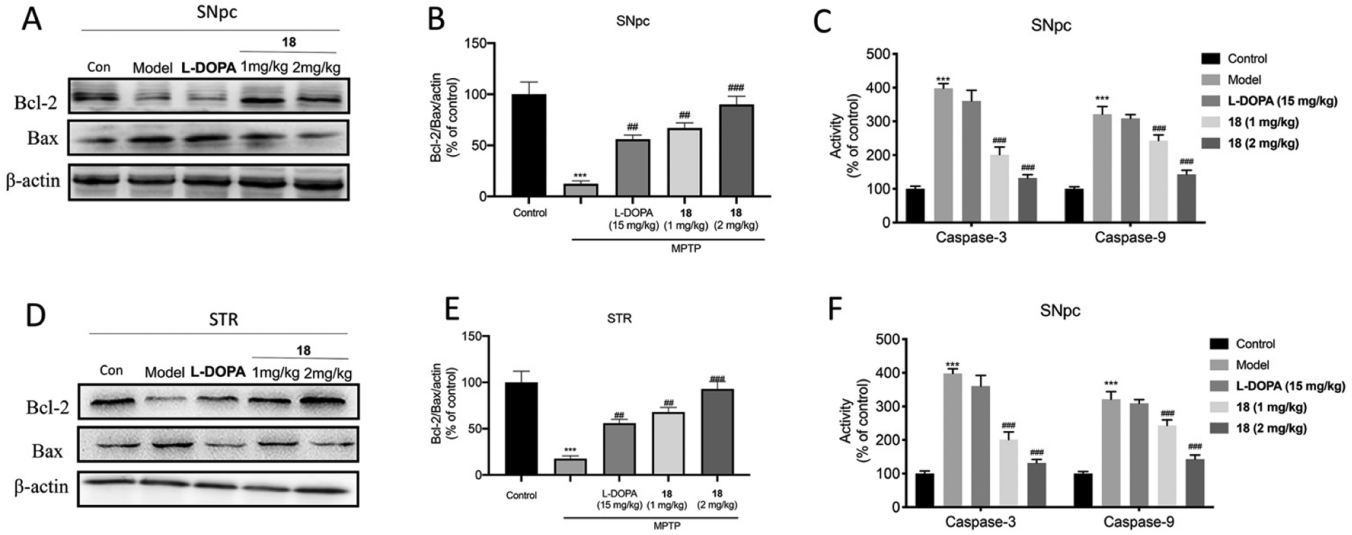

Figure 9. 18 alleviated the apoptosis of the SNpc neuron in the MPTP-induced acute PD model. (A,D) Original bands of Bax and Bcl-2 in SNpc and STR, β-actin served as control. (B,E) Quantitative analysis of blots. (C,F) Caspase-3 and caspase-9 activities in SNpc and STR. All data are presented as means ± SEM. ***p < 0.001, compared with the control group; ##p < 0.01 or ###p < 0.001, compared with the MPTP treatment group.

immunofluorescence histochemistry and enzyme-linked immunosorbent assay. Results showed that **18** can substantially increase the level of GDNF in glial cells compared with the control and MPTP/probenecid groups (Figure 11F). Furthermore, the level of GDNF in the SNpc was also remarkably increased by **18** in a dose-dependent manner (Figure 11G). These data suggested that the therapeutic effect of **18** would most likely promote the secretion of GDNF in glial cells to repair damaged DAergic neurons in the SNpc.

In Vitro ADME/Tox and In Vivo Pharmacokinetic Properties of 18. The drug-like properties of **18** were examined through CYP inhibition and microsomal stability tests. The inhibitory effects of **18** on CYP enzymes (subtypes 2C19, 2D6, 2C9, 1A2, and 3A4) were tested for the possibility of drug−drug interactions. The results are expressed as the percentage of CYP activity that remained after treatment with **18** at 10 μM (Table 2). The stability of **18** was determined from the percentage of the parent compound remaining after 30 min of incubation with human liver microsomes (Table 2). The plasma stability of **18** in mice was also excellent, with 94.2% of the parent compound remaining after 30 min of incubation. In addition, the physicochemical properties of **18** were confirmed to be compatible with beneficial drug-like properties (predicted pK_a = 6.95; c log P = 2.75). A summary of data related to compound **18** are shown in Table 2. In the pharmacokinetic study, we observed that **18** dosed as an oral solution was rapidly absorbed, and its blood and brain concentrations reached the ideal range (Table 3) and were higher than those of **4b**. The results suggested that our structure optimization was successful, and the optimization method can increase the activity and improve the efficacy of **18** in vivo.

Safety Profiles of 18. In the in vivo toxicity study, **18** showed satisfactory maximum tolerated doses with a median lethal dose of 3.45 g/kg after being orally administered to mice. The hematoxylin and eosin (HE) staining of the main viscera (Figure S2) showed that **18** had no detectable adverse effects in the heart, liver, spleen, lung, and kidney at 1000 mg/kg in the 14-day toxicity study. Organ coefficients (Table S3), blood biochemistry analysis (Table S4), body weight (Figure S3), and blood routine analysis (Figure S2) also indicated that **18** can be considered for long-term administration as PD medication.

CONCLUSIONS

Our previous efforts in achieving iNOS inhibitors with excellent potency have led to a class of molecules bearing a scaffold of NPAs. However, their iNOS inhibitory effects and BBB levels still have much room for improvement. This study describes the design, synthesis, and biological activities of a series of NPA derivatives that act as potent selective iNOS inhibitors. First, 209 NPA derivatives were designed, and among these compounds, 20 NPA derivatives (**1**−**20**) with both predicted potent activities, and higher BBB permeability, were finally confirmed to be synthesized through a concise, efficient, and gram-scale method. Some generalities about the SARs of these compounds can be made as the following: (1) the introduction of trifluoromethyl group into the cinnamic acid moiety remarkably increased the activity; (2) NPAs containing aromatic amino acid exhibited better iNOS selectivity than those with aliphatic amino acid. The structure−permeability relationship of these compounds showed that the introduction of the aromatic amino acid and trifluoromethyl group make great contributions to BBB permeability. Notably, the oral administration of **18** at low dosages (1 and 2 mg/kg) demonstrated preventive and therapeutic effects in the MPTP-induced acute PD model and MPTP/probenecid-induced chronic PD model through iNOS inhibition and DAergic neuronal repair pathways. Our study provided evidence supporting **18** as a potential candidate for PD treatment because of its potency in vitro and in vivo, impressive penetration of the BBB, and low toxicity.

EXPERIMENTAL SECTION

General Chemistry. Reagents and solvents were purchased from common commercial suppliers and were used without further purification. Reaction progress was monitored using analytical thin-layer chromatography on precoated silica gel GF_{254} (Qingdao

https://doi.org/10.1021/acs.jmedchem.1c00578
J. Med. Chem. 2021, 64, 7760−7777

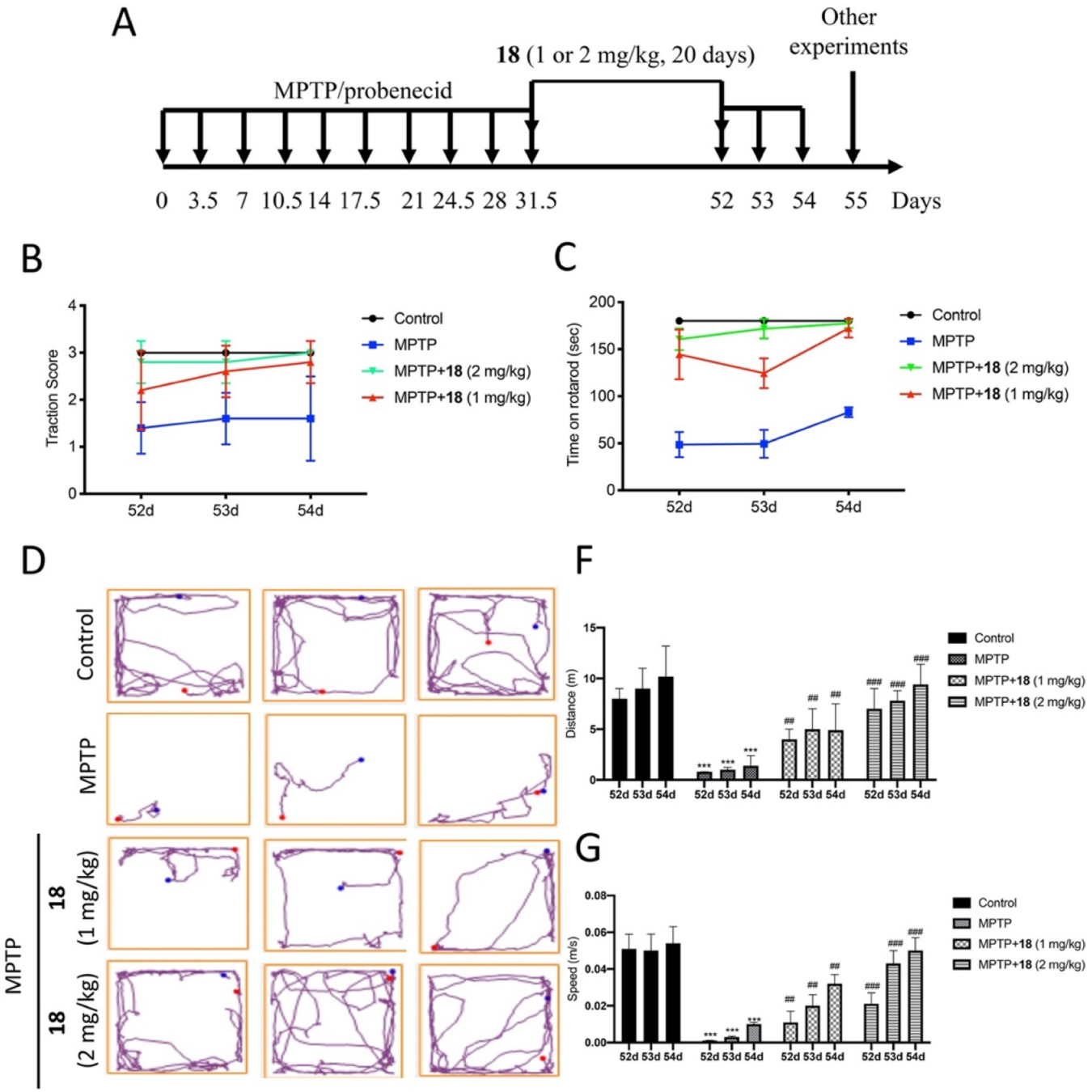

Figure 10. Therapeutic effects of **18** on MPTP/probenecid-induced chronic PD motor deficits. (A) Experimental procedure and drug administration scheme. (B) Traction test. (C) Rotarod test. (D) Motion trail of the first three mice in each group (no. 1, 2, and 3) in the open-field test (n = 8 mice/group). (E) Total distance of mice in the open-field test (n = 8 mice). (F) Mean velocity of mice in the open-field test (n = 8). (F) Mean speed of mice in the open-field test (n = 8). All data are presented as means ± SEM. ***p < 0.001, compared with the control group; ##p < 0.01 or ###p < 0.001, compared with the MPTP treatment group.

Haiyang Chemical Plant, Qingdao, China) plates. The melting point was determined on a XT4MP apparatus (Taike Corp, Beijing, China). ^{1}H and ^{13}C NMR spectra were obtained by a BRUKER AVANCE AV-500 (^{1}H NMR, 500 MHz; ^{13}C NMR, 125 MHz) or by BRUKER AVANCE AV-300 (^{1}H NMR, 300 MHz; ^{13}C NMR, 75 MHz) with DMSO-d_6 as the solvents and TMS as the internal standard. High-resolution electron impact mass spectra (HRMS) are recorded under an Agilent 6520 Q-TOF mass spectrometer (Agilent Technologies, USA). Optical rotations were measured on a Rudolph Autopol IV polarimeter at 20 °C. The purities of all compounds were confirmed to be higher than 95% by the high-performance liquid chromatography (HPLC) method performed with an Agilent 1260 HPLC System.

General Procedure for Synthesis of 1−20. Under a nitrogen atmosphere, $SOCl_2$ (1 mL, 13.75 mmol) was added in portions to a solution of L-amino acid (6 mmol) in methanol (25 mL) at −10 °C within 30 min, and the mixture was warmed to room temperature and stirred for 12 h. After the solvent was removed in vacuum, 80% aqueous ethanol (50 mL) was added to dissolve amino acid methyl ester hydrochloride, and 5.0 mmol corresponding to the substituted cinnamic acid (6 mmol), 4-(4,6-dimethoxy-1,3,5-triazin-2-yl)-4-methyl morpholinium chloride (1.65 g, 5.5 mol), $NaHCO_3$ (500 mg, 6 mmol) was added. The solution was stirred at room

https://doi.org/10.1021/acs.jmedchem.1c00578
J. Med. Chem. 2021, 64, 7760−7777

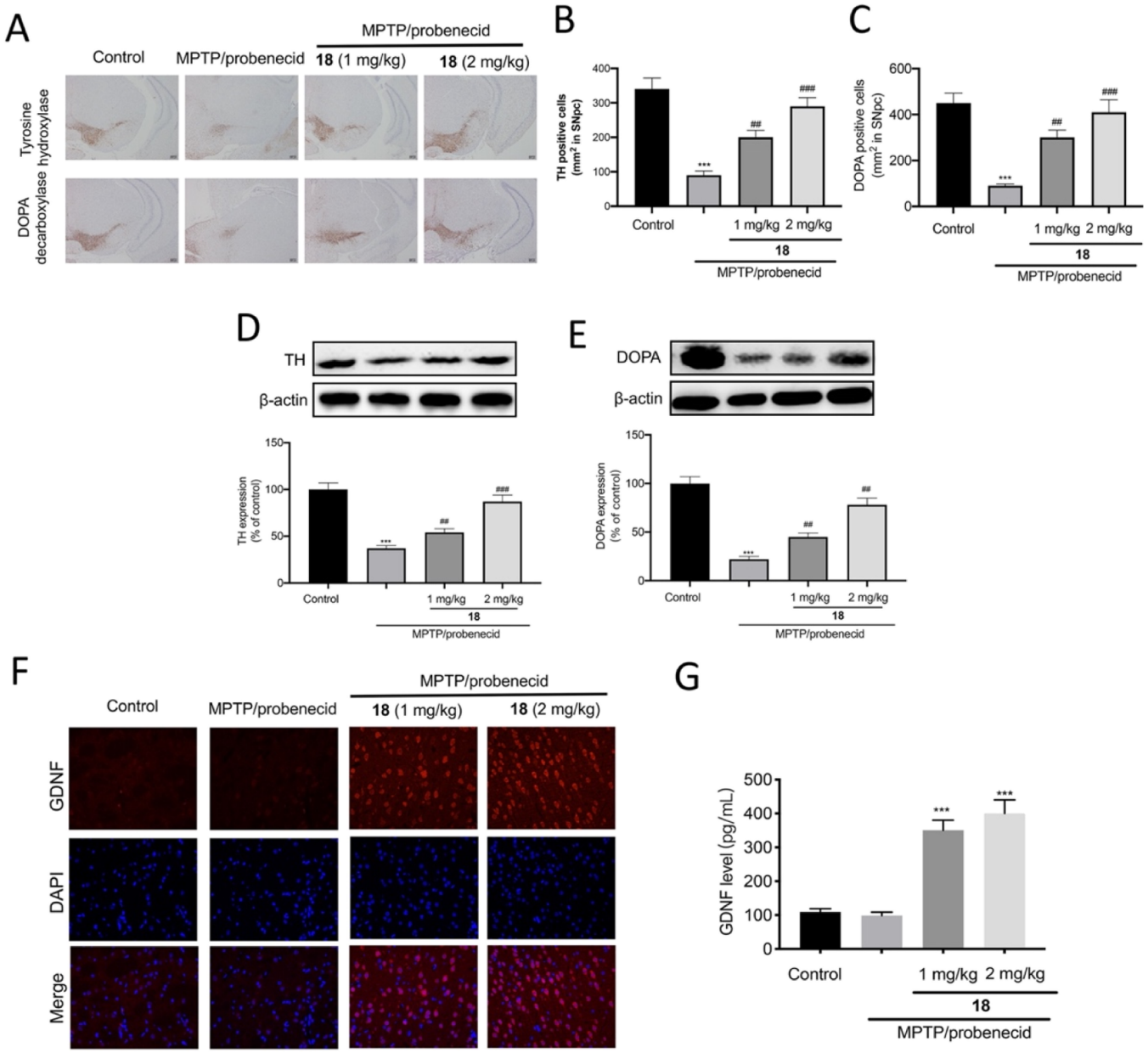

Figure 11. Effects of **18** on the repair of DAergic neurons. (A) Immunohistochemical staining showing TH and DOPA decarboxylase-positive cells in the SN (scale bar: 200 μm). (B,C) Stereological counting of TH and DOPA decarboxylase-positive cells (n = 3). (D) Western blot analysis of the changes in the protein level of TH in SNpc. (E) Western blot analysis of the changes in the protein level of DOPA in SNpc. (F,G) Immunofluorescence staining showing GDNF in microglia of mice. All data are presented as means ± SEM. ***p < 0.001, compared with the control group; ##p < 0.01 or ###p < 0.001, compared with the MPTP treatment group.

temperature for 6 h. The mixture was concentrated and the residue was extracted with EtOAc/H_2O (50 mL × 3). The combined organic layer was washed with a saturated $NaHCO_3$ solution and saturated brine solution, dried over anhydrous Na_2SO_4, and concentrated in vacuum. After recrystallization in PE/EtOAc (5:1−3:1), a series of intermediates, the methyl ester of the target product, were obtained as colorless crystals. The mentioned intermediate was dissolved in 80% aqueous methanol (50 mL), K_2CO_3 (2.075 g, 15 mmol) was added in portions and the solution was stirred at room temperature for 2 h. The mixture was concentrated, and $KHSO_4$ (50 mL, 1 M) aqueous solution was added. The residue was extracted with EtOAc (30 mL × 5), and the combined organic layer was dried over anhydrous Na_2SO_4 and concentrated in vacuum to afford the final product as a white powder.

*2-Chloro-(E)-cinnamoyl]-L-phenylalanine Acid (**1**).* White powder in 46% yield, mp 126−127 °C, $[\alpha]_D^{20}$ −14.7 (c 0.1, MeOH). ^{1}H NMR (500 MHz, DMSO-d_6): δ_H 12.80 (s, 1H), 8.53 (1H, d, J = 7.8 Hz), 7.72 (1H, m), 7.70 (1H, d, J = 15.8 Hz), 7.55 (1H, m), 7.44 (2H, m), 7.33−7.22 (5H, m), 6.80 (1H, d, J = 15.8 Hz), 4.61 (1H, m), 3.16 (1H, dd, J = 6.9, 2.9 Hz), 2.98 (1H, dd, J = 6.9, 5.6 Hz); ^{13}C NMR (125 MHz, DMSO-d_6): δ_C 173.32, 164.88, 138.02, 134.97, 133.77, 133.08, 133.06, 131.46, 129.55 (2C), 128.71 (2C), 128.26, 128.05, 126.95, 125.21, 54.19, 37.31. HRMS (ESI) m/z: $[M + H]^+$ calcd for $C_{18}H_{16}ClNO_3$, 330.0819; found, 330.0889.

*2-Chloro-(E)-cinnamoyl]-L-4-F-phenylalanine Acid (**2**).* White powder in 55% yield, mp 139−140 °C, $[\alpha]_D^{20}$ −15.2 (c 0.1, MeOH). ^{1}H NMR (300 MHz, DMSO-d_6): δ_H 12.83 (1H, s), 8.52 (1H, d, J = 9.0 Hz), 7.73−7.67 (1H, m), 7.69 (1H, d, J = 15.7 Hz), 7.51 (1H, dd, J = 5.8, 3.5 Hz), 7.40 (2H, m), 7.29 (2H, m), 6.76 (1H, d, J = 15.7 Hz), 4.60 (1H, m), 3.14 (1H, dd, J = 13.8, 4.9 Hz), 2.94 (1H, dd, J = 13.8, 9.3 Hz); ^{13}C NMR (75 MHz, DMSO-d_6): δ_C 172.67, 164.35, 162.63, 159.43, 134.49, 133.61, 133.57, 133.28,

https://doi.org/10.1021/acs.jmedchem.1c00578
J. Med. Chem. 2021, 64, 7760−7777

Table 2. Summary of Properties of 18

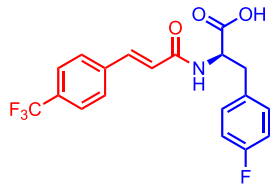

property	value
pK_a, log P (c log P)	4.03 (4.27)
inhibition of iNOS response (IC_{50}, nM)	74
CYP inhibition (% of control activity, 10 μM)[a]	77.4 (2C19), 99.7 (2D6), 96.7 (2C9), 87.2 (1A2), 97.4 (3A4)
human microsomal stability (1 μM)[b]	86.3 (30 min)
plasma stability (% of untreated control)	90.2 (60 min)
PAMPA-BBB (P_e, cms^{-1})	19.02 ± 1.32 (CNS^+)

[a]Cytochrome P450 (CYP) inhibition assay was performed using a P450-Glo assay system (Promega). [b]In vitro microsomal stability of the synthesized compound; % remaining was determined after 30 min of incubation with human microsomes. The % of parent compound remaining is calculated by comparing peak areas.

132.52, 130.93, 130.82, 129.92, 127.70, 127.51, 124.61, 115.00, 114.73, 53.64, 35.92. HRMS (ESI) m/z: $[M + H]^+$ calcd for $C_{18}H_{15}ClFNO_3$, 348.0724; found, 348.0796.

*2-Chloro-(E)-cinnamoyl]-L-leucine Acid (**3**).* White powder in 42% yield, mp 85−87 °C, $[\alpha]_D^{20}$ −16.1 (c 0.1, MeOH). ^{1}H NMR (300 MHz, DMSO-d_6): δ_H 12.59 (1H, s), 8.45 (1H, d, J = 8.0 Hz), 7.74 (1H, d, J = 15.8 Hz), 7.71 (1H, m), 7.53 (1H, m), 7.42 (2H, m), 6.78 (1H, d, J = 15.8 Hz), 4.37 (1H, dd, J = 15.1, J = 8.7 Hz), 1.67−1.58 (3H, m), 0.90 (6H, q, J = 6.3Hz); ^{13}C NMR (75 MHz, DMSO-d_6): δ_C 177.00, 167.45, 137.51, 136.36, 135.72, 134.00, 133.04, 130.84, 130.62, 127.89, 53.57, 27.46, 25.87, 24.39. HRMS (ESI) m/z: $[M + H]^+$ calcd for $C_{15}H_{18}ClNO_3$, 296.0975; found, 296.1046.

*2-Chloro-(E)-cinnamoyl]-L-isoleucine Acid (**4**).* White powder in 53% yield, mp 66−67 °C, $[\alpha]_D^{20}$ −15.5 (c 0.1, MeOH). ^{1}H NMR (500 MHz, DMSO-d_6): δ_H 12.61 (1H, s), 8.34 (1H, d, J = 8.0 Hz), 7.77(1H, d, J = 15.8 Hz), 7.76 (1H, m), 7.55 (1H, br s), 7.45 (2H, m), 6.95 (1H, d, J = 15.7 Hz), 4.37 (1H, t, J = 4.3 Hz), 1.86 (1H, m), 1.48 (1H, m), 1.26 (1H, m), 0.92 (7H, m); ^{13}C NMR (125 MHz, DMSO-d_6): δ_C 173.34, 165.16, 134.88, 133.80, 133.23, 131.40, 130.48, 128.26, 127.99, 125.50, 56.98, 37.01, 25.25, 16.12, 11.77. HRMS (ESI) m/z: $[M + H]^+$ calcd for $C_{15}H_{18}ClNO_3$, 296.0975; found, 296.1046.

*4-Chloro-(E)-cinnamoyl]-L-phenylalanine Acid (**5**).* White powder in 64% yield, mp 221−224 °C, $[\alpha]_D^{20}$ −16.9 (c 0.1, MeOH). ^{1}H NMR (500 MHz, DMSO-d_6): δ_H 12.77 (1H, s), 8.42 (1H, d, J = 7.8 Hz), 7.60 (1H, d, J = 8.0 Hz), 7.49 (1H, d, J = 8.0 Hz), 7.42 (1H, d, J = 15.8 Hz), 7.31−7.23 (6H, m), 6.75 (1H, d, J = 15.8 Hz), 4.62 (1H, dd, J = 7.6, J = 4.9 Hz), 3.17 (1H, dd, J = 8.3, 2.7 Hz), 2.96 (1H, dd, J = 8.3, 5.7 Hz); ^{13}C NMR (125 MHz, DMSO-d_6): δ_C 173.41, 165.16, 138.35, 138.06, 134.45, 134.26, 129.73 (2C), 129.55 (2C), 129.44 (2C), 128.69 (2C), 126.93, 123.02, 54.13, 37.35. HRMS (ESI) m/z: $[M + H]^+$ calcd for $C_{18}H_{16}ClNO_3$, 330.0819; found, 330.1046.

*4-Chloro-(E)-cinnamoyl]-L-4-F-phenylalanine Acid (**6**).* White powder in 64% yield, mp 234−235 °C, $[\alpha]_D^{20}$ −17.7 (c 0.1, MeOH). ^{1}H NMR (500 MHz, DMSO-d_6): δ_H 12.76 (1H, s), 8.42 (1H, d, J = 8.2 Hz), 7.60 (2H, d, J = 8.3 Hz), 7.49 (2H, d, J = 8.3 Hz), 7.41 (1H, d, J = 15.8 Hz), 7.30 (1H, dd, J = 5.3, 3.5 Hz), 7.12 (2H, t, J = 5.3 Hz), 6.73 (1H, d, J = 15.8 Hz), 4.59 (1H, m), 3.14 (1H, dd, J = 8.3, 2.9 Hz), 2.96 (1H, dd, J = 8.3, 5.6 Hz); ^{13}C NMR (125 MHz, DMSO-d_6): δ_C 173.28, 165.15, 162.52, 160.59, 138.38, 134.46, 134.24, 134.19, 131.43, 129.75 (2C), 129.45 (2C), 122.95, 115.47, 115.30, 54.10, 36.47. HRMS (ESI) m/z: $[M + H]^+$ calcd for $C_{18}H_{15}ClFNO_3$, 348.0724; found, 348.0797.

*4-Chloro-(E)-cinnamoyl]-L-leucine Acid (**7**).* White powder in 67% yield, mp 158−159 °C, $[\alpha]_D^{20}$ −18.5 (c 0.1, MeOH). ^{1}H NMR (300 MHz, DMSO-d_6): δ_H 12.58 (1H, s), 8.35 (1H, d, J = 8.0 Hz), 7.59 (2H, d, J = 8.2 Hz), 7.47 (2H, d, J = 8.2 Hz), 7.43 (1H, d, J = 15.8 Hz), 6.74 (1H, d, J = 15.8 Hz), 4.37 (1H, dd, J = 9.0, 6.0 Hz), 1.68−1.55 (3H, m), 0.89 (6H, q, J = 6.2 Hz); ^{13}C NMR (75 MHz, DMSO-d_6): δ_C 177.07, 167.76, 140.84, 136.98, 136.89, 132.62 (2C), 132.26 (2C), 125,66, 53.47, 27.45, 25.87, 24.37. HRMS (ESI) m/z: $[M + H]^+$ calcd for $C_{15}H_{18}ClNO_3$, 296.0972; found, 296.1044.

*4-Chloro-(E)-cinnamoyl]-L-isoleucine Acid (**8**).* White powder in 63% yield, mp 137−138 °C, $[\alpha]_D^{20}$ −19.3 (c 0.1, MeOH). ^{1}H NMR (500 MHz, DMSO-d_6): δ_H 12.58 (1H, s), 8.23 (1H, d, J = 6.8 Hz), 7.61 (2H, br), 7.51 (2H, br), 7.45 (1H, d, J = 15.8 Hz), 6.89 (1H, d, J = 15.8 Hz), 4.37 (1H, t, J = 5.0 Hz), 1.86 (1H, m), 1.48 (1H, m), 1.27 (1H, m), 0.90 (7H, m); ^{13}C NMR (125 MHz, DMSO-d_6): δ_C 173.42, 165.29, 138.20, 134.42, 134.37, 129.67 (2C), 129.46 (2C), 123.30, 56.90, 37.01, 25.23, 16.11, 11.76. HRMS (ESI) m/z: $[M + H]^+$ calcd for $C_{15}H_{18}ClNO_3$, 296.0973; found, 296.1064.

*3,4-Dichloro-(E)-cinnamoyl]-L-phenylalanine Acid (**9**).* White powder in 59% yield, mp 137−138 °C, $[\alpha]_D^{20}$ −14.7 (c 0.1, MeOH). ^{1}H NMR (500 MHz, DMSO-d_6): δ_H 12.79 (1H, s), 8.40 (1H, d, J = 7.8 Hz), 7.86 (1H, s), 7.70 (1H, d, J = 8.3 Hz), 7.58 (1H, d, J = 8.3 Hz), 7.39 (1H, d, J = 15.8 Hz), 7.23 (1H, m), 6.80 (1H, d, J = 15.8 Hz), 4.62 (1H, m), 3.17 (1H, dd, J = 8.3, 3.1 Hz), 2.97 (1H, dd, J = 8.2, 5.6 Hz); ^{13}C NMR (125 MHz, DMSO-d_6): δ_C 173.31, 164.87, 137.98, 137.11, 136.24, 132.17, 131.54, 129.93 (2C), 129.55 (2C), 128.70, 127.81, 126.95, 124.48, 54.11, 37.31. HRMS (ESI) m/z: $[M + H]^+$ calcd for $C_{15}H_{18}ClNO_3$, 364.0429; found, 364.0505.

*3,4-Dichloro-(E)-cinnamoyl]-L-4-F-phenylalanine Acid (**10**).* White powder in 80% yield, mp 153−154 °C, $[\alpha]_D^{20}$ −15.6 (c 0.1, MeOH). ^{1}H NMR (500 MHz, DMSO-d_6): δ_H 12.83 (1H, s), 8.40 (1H, d, J = 8.3 Hz), 7.86 (1H, s), 7.70 (1H, d, J = 5.0 Hz), 7.58 (1H, d, J = 5.0 Hz), 7.40 (1H, d, J = 15.8 Hz), 7.31 (1H, m), 7.13 (1H, m), 6.80 (1H, d, J = 15.8 Hz), 4.60 (1H, m), 3.12 (1H, dd, J = 8.3, 2.8 Hz), 2.93 (1H, dd, J = 8.3, 5.5 Hz); ^{13}C NMR (125 MHz, DMSO-d_6): δ_C 175.77, 167.44, 167.44, 165.73, 139.72, 138.79, 136.70, 136.66, 134.75, 134.10, 134.03, 133.92, 132.50, 130.38, 126.99, 118.10, 117.82, 56.68, 39.04. HRMS (ESI) m/z: $[M + H]^+$ calcd for $C_{18}H_{14}Cl_2FNO_3$, 382.0335; found, 382.0409.

*3,4-Dichloro-(E)-cinnamoyl]-L-leucine Acid (**11**).* White powder in 42% yield, mp 107−109 °C, $[\alpha]_D^{20}$ −16.1 (c 0.1, MeOH). ^{1}H NMR (300 MHz, DMSO-d_6): δ_H 12.60 (1H, s), 8.35 (1H, d, J = 8.0 Hz), 7.85 (1H, br s), 7.68 (1H, d, J = 8.4 Hz), 7.57 (1H, dd, J = 8.4, 1.7 Hz), 7.42 (1H, d, J = 15.8 Hz), 6.78 (1H, d, J = 15.8 Hz), 4.37 (1H, dd, J = 14.6, 8.1 Hz), 1.70−1.55 (3H, m), 0.89 (6H, q, J = 6.3 Hz); ^{13}C NMR (75 MHz, DMSO-d_6): δ_C 176.99, 167.47, 139.59, 138.89, 134.14, 132.51, 130.31, 127.17, 53.51, 27.45, 25.88, 24.38. HRMS (ESI) m/z: $[M + H]^+$ calcd for $C_{15}H_{17}Cl_2NO_3$, 330.0583; found, 330.0656.

*3,4-Dichloro-(E)-cinnamoyl]-L-isoleucine Acid (**12**).* White powder in 54% yield, mp 98−101 °C, $[\alpha]_D^{20}$ −17.7 (c 0.1, MeOH). ^{1}H NMR (500 MHz, DMSO-d_6): δ_H 12.61 (1H, s), 8.22 (1H, d, J = 8.5 Hz), 7.87 (1H, d, J = 2.6 Hz), 7.70 (1H, d, J = 8.5 Hz), 7.58 (1H, dd,

Table 3. Pharmacokinetic Properties of 18 and 4b

	blood			brain		
comp.	$AUC_{0-\infty}$ (h·ng/mL)	$t_{1/2}$ (h)	C_{max} (ng/mL)	$AUC_{0-\infty}$ (h·ng/mL)	$t_{1/2}$ (h)	C_{max} (ng/mL)
4b	3453.5 ± 441.9	1.2 ± 0.3	1004.3 ± 107.2	567.3 ± 43.1	0.9 ± 0.2	40.2 ± 5.1
18	18977.3 ± 1209.2	1.9 ± 0.5	4936.3 ± 267.2	2100.4 ± 100.9	1.7 ± 0.3	578.2 ± 43.1

https://doi.org/10.1021/acs.jmedchem.1c00578
J. Med. Chem. 2021, 64, 7760−7777

J = 8.5, 2.6 Hz), 7.44 (1H, d, J = 15.8 Hz), 6.96 (1H, d, J = 15.8 Hz), 4.35 (1H, dd, J = 5.0, 3.5 Hz), 1.87 (1H, m), 1.49 (1H, m), 1.25 (1H, m), 0.90 (7H, m); ^{13}C NMR (125 MHz, DMSO-d_6): δ_C 173.37, 164.96, 136.86, 136.43, 132.17, 132.08, 131.56, 129.83, 127.75, 124.88, 57.03, 37.09, 25.22, 16.11, 11.79. HRMS (ESI) m/z: [M + H]$^+$ calcd for $C_{15}H_{17}Cl_2NO_3$, 330.0585; found, 330.0655.

*4-Methyl-(E)-cinnamoyl]-L-phenylalanine Acid (**13**).* White powder in 48% yield, mp 135−137 °C, $[\alpha]_D^{20}$ −19.4 (c 0.1, MeOH). ^{1}H NMR (300 MHz, DMSO-d_6): δ_H 12.76 (1H, s), 8.36 (1H, d, J = 8.0 Hz), 7.44 (2H, d, J = 7.4 Hz), 7.36 (1H, d, J = 15.8 Hz), 7.28−7.20 (7H, m), 6.65 (1H, d, J = 15.8 Hz), 4.59 (1H, m), 3.13 (1H, dd, J = 13.8, 4.8 Hz), 2.95 (1H, dd, J = 11.6, 9.5 Hz), 2.31 (3H, s); ^{13}C NMR (75 MHz, DMSO-d_6): δ_C 176.07, 168.08, 142.23, 142.20, 140.68, 135.10, 132.57 (2C), 132.11 (2C), 131.25 (2C), 130.57 (2C), 129.47, 123.72, 56.67, 39.93, 23.97. HRMS (ESI) m/z: [M + H]$^+$ calcd for $C_{19}H_{19}NO_3$, 310.1365; found, 310.1437.

*4-Methyl-(E)-cinnamoyl]-L-4-F-phenylalanine Acid (**14**).* White powder in 52% yield, mp 143−144 °C, $[\alpha]_D^{20}$ −19.7 (c 0.1, MeOH). ^{1}H NMR (500 MHz, DMSO-d_6): δ_H 12.75 (1H, s), 8.37 (1H, d, J = 7.8 Hz), 7.47 (1H, d, J = 8.4 Hz), 7.38 (1H, d, J = 15.8 Hz), 6.97 (1H, d, J = 15.8 Hz), 4.60 (1H, m), 3.14 (1H, dd, J = 8.2, 2.6 Hz), 2.96 (1H, dd, J = 8.2, 5.6 Hz), 2.35 (s, 3H); ^{13}C NMR (125 MHz, DMSO-d_6): δ_C 173.40, 165.52, 160.59, 139.79, 139.68, 134.26, 134.24, 132.24, 131.43, 131.36, 130.00, 128.02, 121.12, 115.46, 115.29, 54.10, 36.51, 21.39. HRMS (ESI) m/z: [M + H]$^+$ calcd for $C_{19}H_{18}FNO_3$, 328.1271; found, 328.1342.

*4-Methyl-(E)-cinnamoyl]-L-leucine Acid (**15**).* White powder in 42% yield, mp 94−96 °C, $[\alpha]_D^{20}$ −20.7 (c 0.1, MeOH). ^{1}H NMR (500 MHz, DMSO-d_6): δ_H 12.55 (1H, s), 8.29 (1H, d, J = 7.8 Hz), 7.48 (2H, d, J = 7.8 Hz), 7.43 (1H, d, J = 15.8 Hz), 7.25 (2H, d, J = 7.8 Hz), 6.70 (1H, d, J = 15.8 Hz), 4.40 (1H, dd, J = 8.5, 4.6 Hz), 2.35 (3H, s), 1.72−1.58 (3H, m), 0.92 (6H, q, J = 3.8Hz); ^{13}C NMR (125 MHz, DMSO-d_6): δ_C 174.61, 165.55, 139.72, 139.56, 132.62, 130.02 (2C), 127.97 (2C), 121.28, 50.87, 24.89, 23.31, 21.81, 21.40. HRMS (ESI) m/z: [M + H]$^+$ calcd for $C_{16}H_{21}NO_3$, 276.1521; found, 276.1593.

*4-Methyl-(E)-cinnamoyl]-L-isoleucine Acid (**16**).* White powder in 62% yield, mp 75−78 °C, $[\alpha]_D^{20}$ −19.9 (c 0.1, MeOH). ^{1}H NMR (500 MHz, DMSO-d_6): δ_H 8.10 (1H, d, J = 7.2 Hz), 7.48 (2H, d, J = 7.8 Hz), 7.40 (1H, d, J = 15.8 Hz), 7.24 (2H, d, J = 7.8 Hz), 6.86 (1H, d, J = 15.8 Hz), 4.32 (1H, dd, J = 4.3, 3.5 Hz), 1.86 (1H, m), 1.49 (1H, m), 1.25 (1H, m), 0.90 (7H, m); ^{13}C NMR (125 MHz, DMSO-d_6): δ_C 173.87, 165.37, 139.52, 139.08, 132.81, 129.97 (2C), 127.94 (2C), 121.96, 57.72, 37.40, 25.27, 21.38, 16.23, 11.90. HRMS (ESI) m/z: [M + H]$^+$ calcd for $C_{16}H_{21}NO_3$, 276.1521; found, 276.1592.

*4-Trifluoromethyl-(E)-cinnamoyl]-L-phenylalanine Acid (**17**).* White powder in 73% yield, mp 222−224 °C, $[\alpha]_D^{20}$ −20.7 (c 0.1, MeOH). ^{1}H NMR (500 MHz, DMSO-d_6): δ_H 12.85 (1H, s), 8.49 (1H, d, J = 8.0 Hz), 7.79 (4H, s), 7.48 (1H, d, J = 15.8 Hz), 7.32−7.23 (6H, m), 6.86 (1H, d, J = 15.8 Hz), 4.60 (1H, m) 3.14 (1H, dd, J = 8.3, 2.9 Hz), 2.94 (1H, dd, J = 8.3, 5.6 Hz); ^{13}C NMR (125 MHz, DMSO-d_6): δ_C 173.36, 164.85, 139.09, 138.07, 137.98, 129.56 (2C), 128.68 (2C), 126.92 (2C), 126.28 (2C), 125.05, 54.22, 37.35. HRMS (ESI) m/z: [M + H]$^+$ calcd for $C_{19}H_{16}F_3NO_3$, 364.1082; found, 364.1154.

*4-Trifluoromethyl-(E)-cinnamoyl]-L-4-F-phenylalanine Acid (**18**).* White powder in 61% yield, mp 236−238 °C, $[\alpha]_D^{20}$ −19.8 (c 0.1, MeOH). ^{1}H NMR (300 MHz, DMSO-d_6): δ_H 12.79 (1H, s), 8.51 (1H, d, J = 8.1 Hz), 7.77 (4H, s), 7.47 (1H, d, J = 15.9 Hz), 7.28 (2H, m), 6.84 (1H, d, J = 15.9 Hz), 4.58 (1H, m), 3.14 (1H, dd, J = 13.9, 4.9 Hz), 2.94 (1H, dd, J = 13.9, 9.3 Hz); ^{13}C NMR (75 MHz, DMSO-d_6): δ_C 175.78, 167.45, 165.72, 162.52, 141.92, 140.63, 136.69, 134.03, 133.92, 132.55, 131.25 (2C), 128.86 (2C), 127.50 (2C), 118.10, 117.82, 56.72, 39.05. HRMS (ESI) m/z: [M + H]$^+$ calcd for $C_{19}H_{15}F_4NO_3$, 382.0988; found, 382.1059.

*4-Trifluoromethyl-(E)-cinnamoyl]-L-leucine Acid (**19**).* White powder in 46% yield, mp 236−238 °C, $[\alpha]_D^{20}$ −15.7 (c 0.1, MeOH). ^{1}H NMR (300 MHz, DMSO-d_6): δ_H 12.60 (1H, s), 8.44 (1H, d, J = 7.9 Hz), 7.78 (4H, s), 7.51 (1H, d, J = 15.8 Hz), 6.85 (1H, d, J = 15.8 Hz), 4.37 (1H, m), 1.70−1.56 (3H, m), 0.90 (6H, q, J = 6.3 Hz); ^{13}C NMR (75 MHz, DMSO-d_6): δ_C 177.00, 167.49, 140.52, 131.21 (2C), 128.33 (2C), 127.66, 53.53, 27.46, 25.88, 24.38. HRMS (ESI) m/z: [M + H]$^+$ calcd for $C_{16}H_{18}F_3NO_3$, 330.1239; found, 330.1311.

*4-Trifluoromethyl-(E)-cinnamoyl]-L-isoleucine Acid (**20**).* White powder in 51% yield, mp 123−125 °C, $[\alpha]_D^{20}$ −16.4 (c 0.1, MeOH). ^{1}H NMR (500 MHz, DMSO-d_6): δ_H 12.63 (1H, s), 8.33 (1H, d, J = 7.8 Hz), 7.80 (4H, s), 7.53 (1H, d, J = 15.8 Hz), 7.02 (1H, d, J = 15.8 Hz), 4.37 (1H, m), 1.88 (1H, m), 1.48 (1H, m), 1.25 (1H, m), 0.92 (7H, m); ^{13}C NMR (125 MHz, DMSO-d_6): δ_C 173.35, 165.03, 139.53, 137.90, 129.84, 129.59, 128.61, 126.31, 126.28, 125.28, 56.95, 37.02, 25.23, 16.11, 11.76. HRMS (ESI) m/z: [M + H]$^+$ calcd for $C_{16}H_{18}F_3NO_3$, 330.1238; found, 330.1311.

Molecular Simulation Study. A docking study was conducted as per our previous study.[17] The iNOS crystal structure (PDB code: 1R35) carries an active site where the standard molecule I58 was preboned as a co-crystal in IR35.[18] The filtered 209 designed compounds were subjected to docking in that active site by the CDOCKER protocol on Discovery Studio 3.0 (DS 3.0) software. The protein preparation protocol had been followed for preparing the protein, and the filtered molecules were docked into the active sites on the prepared protein. During the analysis, -CDOCKER energy for every single conformational pose were chosen as a selection criterion. MD simulations for 100 ns were performed on iNOS without and with EuC at 300 K at the molecular mechanic level using the GROMOS96 43a1 force field in GROMACS. The iNOS-**18** complex was solvated in a cube box of 0.9% NaCl, and the distance between solute and the box was 5 Å. Both the systems were minimized using 1500 steps of the steepest descent for energy minimization. The resulting trajectories were analyzed using *rms* and *rmsf* utilities of GROMACS. The GROMACS 5.1.2 program was used for MD, and all graphs were prepared using GraphPad Prism 8.0 software.

Cellular Thermal Shift Assay and Isothermal Dose−Response Fingerprint. For cellular thermal shift assay (CETSA) and isothermal dose−-response fingerprint (ITDRF) experiments were conducted similar to the previous report.[22,23] Briefly, for CESTA experiments, spleen cells were seeded in 10 cm culture dishes and then, the cells were incubated with **18** (1 μM) in fresh growth medium) for 3 h at 37 °C with an atmosphere of 95% air and 5% CO_2. The same volume of DMSO was used for a negative control in another 10 cm dish. Subsequently, the medium was removed, and the cells were washed with phosphate-buffered saline (PBS) and distributed into five different microtubes with 80 μL of cell suspension in each tube for both **18** and DMSO-treated cells. The microtubes were heated at the designated temperature (37 to 73 °C) for 4 min on a heating block. After heating, the microtubes were removed and balanced at 25 °C for another 3 min. Then, the cells were lysed to extract the proteins, separated by sodium dodecyl-sulfate polyacrylamide gel electrophoresis, followed by transfer to a poly(vinylidene difluoride) membrane for western blot analysis. For $ITDRF_{CETSA}$ experiments, all procedures are the same as CETSA, and just the cells were incubated with **18** in different concentrations at designated temperatures.

Surface Plasmon Resonance Assay. Surface plasmon resonance (SPR) experiments were performed to investigate the binding affinity between **18** and human recombinant protein iNOS. The procedures were conducted as previously reported with some modifications.[24] Briefly, purified human recombinant protein iNOS (final concentration: 15 μg/mL) was loaded into the chip at 0.5 μL/s in NaAc buffer (pH 5.5) for 20 min at 4 °C. Then, different concentrations of **18** (10 mM stock solution in DMSO) in PBS flowed through the surface of the chip at 0.5 μL/s in PBST (pH 7.4) for 600 s at 4 °C. Finally, the proteins were dissociated from the chip at 2 μL/s in glycine−HCl (pH 2.0) for 360 s at 4 °C. The binding signals (RU) were detected by SPR using a Biacore T200 (GE Healthcare, USA). The RU responses of test compounds with purified recombinant protein iNOS were recorded and ranked, and the binding curve and affinity data were calculated by the system according to the Langmuir binding model.

https://doi.org/10.1021/acs.jmedchem.1c00578
J. Med. Chem. 2021, 64, 7760−7777

Cell Culture. The immortalized murine microglial cell line BV-2 cells and human neuroblastoma SH-SY5Y cells were routinely maintained in Dulbecco's modified Eagle's medium (DMEM) with 10% fetal bovine serum (FBS), supplemented with 100 U/mL penicillin and 100 μg/mL streptomycin at 37 °C in a humidified atmosphere of 95% air and 5% CO_2. All reagents for cell culture were purchased from Invitrogen (CA, USA).

Animals. Male C57BL/6 mice (6−8 weeks old, weighing 20−22 g) were purchased from Comparative Medicine Center (Yangzhou University, China). Mice were acclimatized for 7 days before use. All animals were maintained under a standard housing environment at a temperature of 22−25 °C and kept on a 12 h light−dark cycle and were allowed free access to food and water. All experimental procedures were approved by the Ethical Committee of the China Pharmaceutical University (no. SYXK2016-0011).

NO Production Assay. For the compound screening experiments, the cells were plated in 96-well plates at a density of 5×10^3 cells/well and 24 h later were treated with compounds **1**−**20** or **4b** at 1 μM. Then, 6 h later the cells were treated with LPS (500 ng/mL) and incubated for another 24 h, and the culture media were collected for the detection of the NO inhibition using a commercial NO detection kit (Beyotime, China) at 540 nm (microplate reader, TECAN, Infinite M200, Austria).

NOS Enzyme Inhibition Assay. The inhibitory effect of compounds **1**−**20** on NOS isoforms were evaluated mainly according to previous studies.[32,33] Compounds **1**−**20** were evaluated for their abilities to inhibit human iNOS, eNOS, and nNOS (which were purchased from Abcam) mediated the conversion of [^{3}H]arginine to [^{3}H]citrulline. Various concentrations of compounds (0.01−10 μM) were incubated with 10 nM [^{3}H]arginine and [^{14}C]citrulline (80−120 nM) as an internal standard, cofactors (1.4 mM β-NADP$^+$, 3.0 mM glucose-6-phosphate (G6P), 3.4 mM $MgCl_2$, 0.4 U/mL G6P dehydrogenase, 5.0 μM FAD, 5.0 μM FMN, 5.0 μM BH_4), and enzyme in 100 μL of 50 mM HEPES buffer for 1 h at 37 °C. For eNOS and nNOS assays, additional cofactors 25 nM calmodulin, 0.5 mM $CaCl_2$, and 3.5 mM glutathione were included in the reactions. The reactions were stopped by the addition of 25 μL of 1 M MES and filtered through a AG-50W-X8 (200−400 mesh, Na form) cation exchange resin that had been loaded onto 96-well filter plates using a 100 μL column loader (Millipore). Then, the filtrate was rinsed with 75 and 25 μL ddH_2O, respectively, and the filtrate was collected and the radioactivity in the filtrate was counted. Background activity was determined in the presence of 10 μM AMT. Dose−response curves were drawn according to eight test concentrations (0.01−10 μM), and IC_{50} values were calculated by GraphPad Prism 8.0 (for macOS) and were from a single experiment that was repeated three times with similar results. The calculated standard deviations from dose−response curves of the assays were less than 10% with all NOSs.

D-QSAR Study. Among all the 20 compounds, 80% (i.e., 16) were utilized as a training set for QSAR modeling and the remaining 20% (i.e., 4) were chosen as an external test subset for validating the reliability of the QSAR model by the diverse molecules protocol in DS 3.0 software. The inhibitory activity of the compounds [IC_{50} (μM)] was initially changed into the minus logarithmic scale [IC_{50} (μM)] and then used for subsequent QSAR analysis as the response variable. QSAR models were built by using the create 3D QSAR model protocol in DS 3.0.

PAMPA-BBB Assay. The PAMPA-BBB assay was performed as per previous study.[34] Briefly, the assay was conducted in 10 mM PBS buffer (PH 7.4), and compounds were tested at a concentration of 200 μM. The donor plate was first coated with 4 μL of the porcine brain lipid (20 mg/mL in dodecane), followed by an addition of 250 μL of a test compound. The acceptor plate was filled with 250 μL of PBS, and the donor plate was carefully placed on top of the acceptor plate to make a "sandwich". The plate was incubated at 25 °C for 17 h in a saturated humidity atmosphere with an orbital agitation at 100 rpm. After that, 150 μL of the test solution was collected from each well from both sides (donor and acceptor) and transferred to the UV plate for measurement. The effective permeability (P_e) was calculated by the equation: $P_e = \frac{2.303}{A(t-\tau_{ss})} \cdot \frac{V_A \cdot V_D}{(V_A + V_D)} \cdot \lg\left[1 - \left(\frac{V_A + V_D}{(1-R)\cdot V_D}\right)\left(\frac{C_{A(t)}}{C_{D(0)}}\right)\right]$, where P_e is the effective permeability (cm s^{-1}); V_A and V_D are the volumes of the acceptor and donor wells (0.25 cm^3), respectively; $C_{A(t)}$ is the concentration of the acceptor well at time t; $C_{D(0)}$ and $C_{D(t)}$ are the concentrations of the donor well at t_0 and t, respectively; A is the filter well area (0.21 cm^2); t is the incubation time (s); τ_{ss} is the time to reach a steady state (usually very short compared with the incubation time); and R is the retention membrane factor and was calculated using the following equation: $R = \left[1 - \frac{C_{D(t)}}{C_{D(0)}} - \frac{V_A}{V_D} \cdot \frac{C_{A(t)}}{C_{D(0)}}\right]$. P_e was reported as an average of a triplicate with a standard deviation.

Cell Medium Collection. BV-2 cells (1×10^4 cells/well in a 24-well plate) were pre-treated with **18** (0.1, 1, and 10 μM) for 2 h and then stimulated with LPS (500 ng/mL) for 24 h. The culture media were collected as CM after centrifugation at 2000 rpm for 5 min.

Cell Viability and LDH Release Assays. SH-SY5Y cells (1×10^4 cells/well in a 96-well plate) were seeded 24 h before the CM test. The CM from LPS-stimulated cells was added to SH-SY5Y cells, which were further incubated at 37 °C for 24 h, and then the supernatant was collected to detect the LDH release using the LDH cytotoxicity assay kit (Beyotime, China), and cell viability was measured using the CCK8 assay according to the kit specifications (Dojindo Laboratories, Japan).

Hoechst 33258 Staining and Annexin V−PI Double Staining. SH-SY5Y cells (2×10^5 cells/well in a 6-well plate) were seeded 24 h before the CM test. The CM from LPS-stimulated cells was added to SH-SY5Y cells, which were further incubated at 37 °C for 24 h. For Hoechst 33258 staining (Beyotime, China), the cells were washed with cold PBS three times, and then added Hoechst 33258 (final concentration of 5 μg/mL) for 30 min. After that, cells were washed with cold PBS three times. Finally, images were obtained using a fluorescence microscope (Ts-100, Nikon, Japan). For annexin V−PI double staining, the cells were washed with cold PBS three times and were adjusted to the density of 1×10^6 cells/mL with binding buffer. Then, the staining assay was conducted according to the kit (BD Pharmingen, USA). Finally, all samples were detected by a flow cytometer (Becton Dickin-son, NJ, USA).

Establishment of the MPTP-Induced Acute PD Model and Drug Treatment. 40 C57BL/6 mice were randomly divided into five groups (n = 8 mice/group), including the control group, MPTP-treated group, MPTP + L-DOPA (15 mg/kg, i.g.) group, MPTP + **18** (1 mg/kg, i.g.) group, and MPTP + **18** (2 mg/kg, i.g.) group and allowed 3 days to acclimate before any treatments. DI water containing 0.5% CMC-Na and 1% Tween 80 was used to dissolve **18** and L-DOPA. From day 1 to day 3, for all mice behavior training was conducted. Then, **18** and L-DOPA were pre-administered daily for 10 days (day 4 to day 13). The control group and model group were administered equal volumes of the blank solvent. At day 14, four intraperitoneally (i.p.) injections of MPTP hydrochloride (20 mg/kg) were administered to mice at 2 h intervals a day. After the last MPTP injection, the mice were subjected to the rotarod test, traction test, and open-field test at different time points. 10 days later after MPTP injection, SNpc and STR were collected to perform western blot, immunohistochemistry, and the other biochemical criterion detection.

Establishment of the MPTP/Probenecid-Induced Chronic PD Model and Drug Treatment. 32 C57BL/6 mice were randomly divided into four groups (n = 8 mice/group), including control group, MPTP/probenecid-treated group, MPTP/probenecid + **18** (1 mg/kg, i.g.) group, and MPTP/probenecid + **18** (2 mg/kg, i.g.) group and allowed 3 days to acclimate before any treatments. DI water containing 0.5% CMC-Na and 1% Tween 80 was used to dissolve **18**. From day 1 to day 32, the mice were administered MPTP hydrochloride (25 mg/kg in saline) in combination with probenecid (250 mg/kg in DMSO, ip) every three-and-a-half days. After the last MPTP/prob injection, the mice were continually treated daily with **18** (1 or 2 mg/kg) for the next 20 days. Then, the traction test, rotarod test, and open-field test were conducted from day 52 to day 54 to

https://doi.org/10.1021/acs.jmedchem.1c00578
J. Med. Chem. 2021, 64, 7760−7777

evaluate the therapeutic effects of **18** on PD. At day 55, all mice were sacrificed to perform further biochemical detections.

Traction Test.[35] Traction test was performed as a previous study to assess the limb impairment. Mice were hung from a horizontal wire by its forepaws. The mouse was scored 3 points if it grasped the wire with both hind paws, and 2 points if it grasped the wire with one hind paw, and 1 point if it did not grasp the wire with either hind paws. The average time of three tests was calculated for statistical analyses.

Rotarod Test.[35] The rotarod test was performed as our previous study using a rotary rod apparatus. All mice were pre-trained for 3 days prior to drug administration. The training consisted of three consecutive runs with a gradual increase in rpm up to a maximum 25 rpm until the mice were able to keep themselves without falling from the rotary rod for up to 180 s. The average time of three tests was calculated for statistical analyses.

Open-Field Test.[36] Spontaneous locomotor activity was assessed using the open-field test with an automatic recording open-field working station (ZhongShi, Beijing, China). Mice were placed individually in an acrylic apparatus (30 cm × 30 cm × 15 cm) with a floor divided into 6 × 6 cm equal squares in order to explore the arena. The arena was cleaned with 75% ethanol solution and let dry after testing each mouse to avoid the presence of olfactory cues. Total distance and mean velocity were analyzed over a period of 5 min.

Detection of the NO Level, DA Level, and GDNF Level. Brains were removed to strip the SNpc and STR. Samples were homogenized and centrifuged at 2000*g* for 15 min at 4 °C to separate the supernatant. The concentrations of GDNF and DA were measured by the enzyme-linked immunosorbent assay kits (CUSA-BIO, Wuhan, China) and the NO level was measured by Griess Reagent (Beyotime, China); the procedures followed the instructions.

Histochemical Analysis. The TH and DOPA decarboxylase immunohistochemical analyses were performed as previously described. Briefly, brains were removed and cut into 30 μm sections using a freezing microtome (Microm, Walldorf, Germany), and the coronal sections through the substantia nigra (SNpc) and STR were processed. The sections were incubated with primary antibodies against TH or DOPA decarboxylase (Abcam, MA, USA) and the labeled proteins were visualized using 0.06% hydrogen peroxidase and 0.05% 3,3′-diaminobenzidine. After DAB staining, the sections were observed using a light microscope (Nikon, Ts-100, Japan), and the number of positively stained cells in each group was recorded.

Fluorescence Immunohistochemistry. The sections were incubated with the following primary antibody GDNF: a polyclonal rabbit anti-GDNF (Abcam, MA, USA) with a dilution of 1:100 dilution. After incubation, the sections were then incubated with the following secondary antibodies: Alexa Fluor 488 rabbit anti-mouse (1:1000 dilution; Abcam, MA, USA). The sections were counter-stained with 4′,6-diamidino-2-phenylindole dihydrochloride (DAPI; KeyGen, China). Each section was analyzed microscopically (Nikon, Ts-100, Japan).

Western Blot Analysis. The western blot analysis was conducted as per our previous study.[17] Briefly, at the end of the last day, brains were removed to strip the SNpc and STR. Then, the SNpc and STR were adequately lysed in RIPA (100 mg tissue/mL PBS). Then, the BCA assay (Beyotime, China) was used to adjust the concentration of each sample protein to 3 mg/mL. Equal amounts of protein extracts (30 μg) were subject to immunoblot analysis using primary antibodies (all in 1:1000 dilution) followed by secondary antibodies (1:5000 dilution). All the antibodies were purchased from Abcam (MA, USA). The exposure was conducted by a chemiluminescence apparatus (Tanon 5200, China).

CYP Inhibition Assay. CYP inhibition was conducted using a P450-Glo screening system (Promega, Corp.) according to the instructions (Promega Technical Bulletin, P540-Glo). Briefly, the CYP enzyme and the substrate were mixed in KH_2PO_4 buffer (100 mM, pH 7.4) with or without **18** (10 μM), and the reaction was initiated by the addition of the NADPH regeneration system (containing $NADP^+$, $MgCl_2$, G6P, and G6P dehydrogenase). After incubation for 10−30 min at 37 °C (different incubation times depending on the CYP isotype), the reconstituted luciferin detection reagent was added to stop the reaction and generate the luminescent signal. After incubation for 20 min to stabilize the luminescence, signals were detected using a microplate reader (TECAN, Infinite M200, Austria); the inhibition of each CYP isotype by **18** was expressed as the percentage of activity versus control.

Human Microsomal Stability. Human liver microsomes (0.5 mg/mL) were preincubated with **18** at 1 μM in 0.1 M phosphate buffer (pH 7.4) at 37 °C for 5 min before adding the NADPH regeneration buffer (ditto). The incubation was started by treating the NADPH regeneration buffer and terminating with chlorpropamide in acetonitrile after 30 min at 37 °C. Precipitated proteins were removed by centrifugation for 5 min at 14,000*g* at 4 °C. The supernatant was injected into a liquid chromatography/mass spectrometry (LC−MS) system and analyzed using a Shimadzu Nexera XR system (Shimadzu Corporation, Kyoto, Japan). The HPLC column was a Luna C_{18} column (2.0 × 5 mm, 4.6 μm), and the mobile phase was distilled water (A) containing 0.1% formic acid and acetonitrile (B) containing 0.1% formic acid. Data analysis was performed using Xcalibur 1.6 software. The percentage of remaining **18** was calculated by comparing the peak area.

Plasma Stability. In vitro stability of **18** was carried out with an initial concentration of 1000 ng/mL in the rat plasma at 37 °C. A 100 μL of plasma was aliquoted from the incubation solution at 0.5 h, followed by solid-phase extraction. 10 μL of supernatant of each sample was injected into a LC−MS system and analyzed using a Shimadzu Nexera XR system (Shimadzu Corporation, Kyoto, Japan). The HPLC column was a Luna C_{18} column (2.0 × 5 mm, 4.6 μm), and the mobile phase was distilled water (A) containing 0.1% formic acid and acetonitrile (B) containing 0.1% formic acid. Data analysis was performed using Xcalibur 1.6 software. The percentage of remaining **18** was calculated by comparing the peak area.

Pharmacokinetic Analysis. Male BALB/c mice were randomly divided into two groups, including the control group and the drug treatment group. After 16 h of fasting, mice in the drug treatment group were intragastrically administered **18** at a single dose of 30 mg/kg, while the control group were given the same volume of the blank solvent. Then, blood samples and brain samples were collected at 5, 10, 15, and 30 min and 1, 2, 6, 8, 12, and 24 h after dosing, following the decapitation of the animal. The plasma was prepared by centrifuging the blood at 5000 rpm for 10 min and the brains were homogenized with saline, centrifuged at 10,000*g* for 10 min, and then the supernatant was collected. After that, 300 μL of methyl alcohol was added to 300 μL of plasma or brain supernatant, and vortexed 3 min, centrifuged at 10,000*g* for 10 min, and then the supernatant was collected. Then, a 5 μL aliquot of the plasma or brain extract was injected into the LC−MS system on a Shimadzu LCMS-2020 single quadrupole system (Shimadzu Scientific Instruments Inc., Japan). For the detection of **18** and **4b**, an isocratic chromatographic procedure was used with a mobile phase of 40% acetonitrile (0.1% formic acid) and 65% acetonitrile (0.1% formic acid), respectively, at a flow rate of 0.5 mL/min. The chromatographic procedure was performed using the Agilent SB-C18 column (2.1 × 50 mm, 1.8 μm, Agilent Technologies, USA) at 30 °C.

In Vivo Toxicity Assessment. Male BALB/c mice were administered (i.g.) with **18** at 500, 1000, 2000, and 3000 mg/kg for 14 consecutive days. During the 14 days, the mortality of each group (n = 12 mice/group) was counted. At the 15th day, the mice (1000 mg/kg group) were killed, and the blood was collected to conduct blood biochemical analysis (Siemens, ADVIA 2120I, Germany), and the main viscera, including the heart, liver, spleen, lung, and kidney, were removed to perform HE staining.

HE Staining. HE staining was conducted as per a previous study. Briefly, the heart, liver, spleen, lung, and kidney were collected to be cut into 30 μm sections using a freezing microtome (Microm, Walldorf, Germany). Then, the HE staining was performed on the sections according to the kit's specification (KeyGEN BioTECH, China).

Statistical Analysis. The data were expressed as mean ± SD or SEM and analyzed using a one-way analysis of variance (ANOVA),

https://doi.org/10.1021/acs.jmedchem.1c00578
J. Med. Chem. 2021, 64, 7760−7777

followed by Dunnett's post hoc test. $p < 0.05$ was considered statistically significant.

■ ASSOCIATED CONTENT

Supporting Information

The Supporting Information is available free of charge at https://pubs.acs.org/doi/10.1021/acs.jmedchem.1c00578.

Structure characterization of compounds **1**−**20** by ^{1}H NMR, ^{13}C NMR, and ESI/HRMS spectroscopy; HPLC analysis of compounds **1**−**20**; chemical structures of 209 designed compounds; docking scores (-kcal/mol) and BBB level prediction of 209 compounds; organ coefficients and blood biochemistry analysis; correlation coefficient R2; H−E staining of main viscera; and effects of **18** on the body weight and hemocyte number (PDF)

Molecular string files for compounds **1**−**20** (CSV)

Compound **18** with 1R35 (PDB)

■ AUTHOR INFORMATION

Corresponding Authors

Fei Xiong − *State Key Laboratory of Bioelectronics, Jiangsu Laboratory for Biomaterials and Devices, Southeast University, Nanjing 210009, People's Republic of China;* orcid.org/0000-0002-3680-4292; Phone: +86-25-83792496; Email: xiongfei@seu.edu.cn

Hao Wang − *State Key Laboratory of Natural Medicines, School of Traditional Chinese Pharmacy, China Pharmaceutical University, Nanjing 210009, People's Republic of China;* orcid.org/0000-0003-3994-9806; Phone: +86-25-83271328; Email: wanghao@cpu.edu.cn

Authors

Xiao-Long Hu − *State Key Laboratory of Natural Medicines, School of Traditional Chinese Pharmacy, China Pharmaceutical University, Nanjing 210009, People's Republic of China*

Xian-Yu Lv − *State Key Laboratory of Natural Medicines, School of Traditional Chinese Pharmacy, China Pharmaceutical University, Nanjing 210009, People's Republic of China*

Rong Wang − *State Key Laboratory of Natural Medicines, School of Traditional Chinese Pharmacy, China Pharmaceutical University, Nanjing 210009, People's Republic of China*

Huan Long − *State Key Laboratory of Natural Medicines, School of Traditional Chinese Pharmacy, China Pharmaceutical University, Nanjing 210009, People's Republic of China*

Jia-Hao Feng − *State Key Laboratory of Natural Medicines, School of Traditional Chinese Pharmacy, China Pharmaceutical University, Nanjing 210009, People's Republic of China*

Bao-Lin Wang − *State Key Laboratory of Natural Medicines, School of Traditional Chinese Pharmacy, China Pharmaceutical University, Nanjing 210009, People's Republic of China*

Wei Shen − *State Key Laboratory of Natural Medicines, School of Traditional Chinese Pharmacy, China Pharmaceutical University, Nanjing 210009, People's Republic of China*

Hao Liu − *State Key Laboratory of Natural Medicines, School of Traditional Chinese Pharmacy, China Pharmaceutical University, Nanjing 210009, People's Republic of China*

Xiao-Qi Zhang − *Institute of Traditional Chinese Medicine and Natural Products, Jinan University, Guangzhou 510632, People's Republic of China;* orcid.org/0000-0002-4436-0273

Wen-Cai Ye − *Institute of Traditional Chinese Medicine and Natural Products, Jinan University, Guangzhou 510632, People's Republic of China;* orcid.org/0000-0002-2810-1001

Complete contact information is available at: https://pubs.acs.org/10.1021/acs.jmedchem.1c00578

Notes

The authors declare no competing financial interest.

■ ACKNOWLEDGMENTS

Financial support from the China Postdoctoral Science Foundation (nos. 2019M662006, 2019TQ0357), the National Natural Science Foundation of China (nos. 81973206 and 82073804), the Major National Science and Technology Projects of the Chinese 13th five-year plan (no. 2017ZX09309024), the Jiangsu Province Graduate Student Training Innovation Project (no. KYLX16_1208), and the Pharmaceutical Top-Notch Innovative Talent Training Program of China Pharmaceutical University is acknowledged.

■ ABBREVIATIONS

ANOVA, analysis of variance; BBB, blood−brain barrier; CETSA, cellular thermal shift assay; CM, culture medium; CNS, central nervous system; COMT, catechol-*O*-methyltransferase; DA, dopamine; DS, Discovery Studio; DMEM, Dulbecco's modified Eagle's medium; DAPI, 4′,6-diamidino-2-phenylindole dihydrochloride; DMTMM, 4-(4,6-dimethoxy-1,3,5-triazin-2-yl)-4-methylmorpholinium chloride; eNOS, endothelial nitric oxide synthase; FBS, fetal bovine serum; GDNF, glial cell line-derived neurotrophic factor; HE, hematoxylin−eosin; iNOS, inducible nitric oxide synthase; MPTP, 1-methyl-4-phenyl-1,2,3,6-tetrahydropyridine; MAO-B, monoamine oxidase type B; NPAs, *N*-phenylpropenoyl-L-amino acids; NOS, nitric oxide synthase; nNOS, neuronal nitric oxide synthase; PD, Parkinson's disease; QSAR, quantitative structure−activity relationship; RMSF, root-mean-square fluctuations; RMSD, root-mean-square deviation; STR, striatum; SNpc, substantia nigra pars compacta; SARs, structure−activity relationships; TH, tyrosine hydroxylase

■ REFERENCES

(1) Lozano, A. M.; Lang, A. E.; Hutchison, W. D.; Dostrovsky, J. O. New developments in understanding the etiology of Parkinson's disease and in its treatment. *Curr. Opin. Neurobiol.* **1998**, *8*, 783−790.

(2) Ferreira, J. J.; Rocha, J.-F.; Falcão, A.; Santos, A.; Pinto, R.; Nunes, T.; Soares-da-Silva, P. Effect of opicapone on levodopa pharmacokinetics, catechol-O-methyltransferase activity and motor fluctuations in patients with Parkinson's disease. *Eur. J. Neurol.* **2015**, *22*, 815.

(3) Schapira, A. H. V. Monoamine oxidase B inhibitors for the treatment of Parkinson's disease: a review of symptomatic and potential disease-modifying effects. *CNS Drugs* **2011**, *25*, 1061−1071.

(4) Huot, P.; Johnston, T. H.; Lewis, K. D.; Koprich, J. B.; Reyes, M. G.; Fox, S. H.; Piggott, M. J.; Brotchie, J. M. UWA-121, a mixed dopamine and serotonin re-uptake inhibitor, enhances L-DOPA anti-parkinsonian action without worsening dyskinesia or psychosis-like behaviours in the MPTP-lesioned common marmoset. *Neuropharmacology* **2014**, *82*, 76−87.

(5) Chen, J.; Hong, J.; Chunfeng, L. Effect of dopamine agonists versus levodopa as initial treatment in Parkinson's Disease. *Mov. Disord.* **2018**, *33*, S168.
(6) Connolly, B. S.; Lang, A. E. Pharmacological treatment of Parkinson disease: a review. *J. Am. Med. Assoc.* **2014**, *311*, 1670−1683.
(7) Beitz, J. M. Parkinson's disease: a review. *Front. Biosci.* **2014**, *S6*, 65−74.
(8) Rodrigues, L. S.; Fagotti, J.; Targa, A.D. S.; Noseda, A. C. D.; Ilkiwa, J. L.; Chuproski, A. P. Potential new therapies against a toxic relationship: neuroinflammation and Parkinson's disease. *Behav. Pharmacol.* **2019**, *30*, 676−688.
(9) Conti, A.; Miscusi, M.; Cardali, S.; Germanò, A.; Suzuki, H.; Cuzzocrea, S.; Tomasello, F. Nitric oxide in the injured spinal cord: synthases cross-talk, oxidative stress and inflammation. *Brain Res. Rev.* **2007**, *54*, 205−218.
(10) Hague, S.; Peuralinna, T.; Eerola, J.; Hellstrom, O.; Tienari, P. J.; Singleton, A. B. Confirmation of the protective effect of iNOS in an independent cohort of Parkinson disease. *Neurology* **2004**, *62*, 635−636.
(11) Hunot, S.; Boissière, F.; Faucheux, B.; Brugg, B.; Mouatt-Prigent, A.; Agid, Y.; Hirsch, E. C. Nitric oxide synthase and neuronal vulnerability in Parkinson's disease. *Neuroscience* **1996**, *72*, 355−363.
(12) Broom, L.; Marinova-Mutafchieva, L.; Sadeghian, M.; Davis, J. B.; Medhurst, A. D.; Dexter, D. T. Neuroprotection by the selective iNOS inhibitor GW274150 in a model of Parkinson disease. *Free Radical Biol. Med.* **2011**, *50*, 633−640.
(13) Iravani, M. M.; Kashefi, K.; Mander, P.; Rose, S.; Jenner, P. Involvement of inducible nitric oxide synthase in inflammation-induced dopaminergic neurodegeneration. *Neuroscience* **2002**, *110*, 49−58.
(14) Dehmer, T.; Lindenau, J.; Haid, S.; Dichgans, J.; Schulz, J. B. Deficiency of inducible nitric oxide synthase protects against MPTP toxicity in vivo. *J. Neurochem.* **2000**, *74*, 2213−2216.
(15) Okuno, T.; Nakatsuji, Y.; Kumanogoh, A.; Moriya, M.; Ichinose, H.; Sumi, H.; Fujimura, H.; Kikutani, H.; Sakoda, S. Loss of dopaminergic neurons by the induction of inducible nitric oxide synthase and cyclooxygenase-2 via CD 40: relevance to Parkinson's disease. *J. Neurosci. Res.* **2005**, *81*, 874−882.
(16) Minhas, R.; Bansal, Y.; Bansal, G. Inducible nitric oxide synthase inhibitors: A comprehensive update. *Med. Res. Rev.* **2020**, *40*, 823−855.
(17) Hu, X.-L.; Lin, J.; Lv, X.-Y.; Feng, J.-H.; Zhang, X.-Q.; Wang, H.; Ye, W.-C. Synthesis and biological evaluation of clovamide analogues as potent anti-neuroinflammatory agents in vitro and in vivo. *Eur. J. Med. Chem.* **2018**, *151*, 261−271.
(18) Hallinan, E. A.; Kramer, S. W.; Houdek, S. C.; Moore, W. M.; Jerome, G. M.; Spangler, D. P.; Stevens, A. M.; Shieh, H. S.; Manning, P. T.; Pitzele, B. S. 4-Fluorinated L-lysine analogs as selective i-NOS inhibitors: methodology for introducing fluorine into the lysine side chain. *Org. Biomol. Chem.* **2003**, *1*, 3527−3534.
(19) Cinelli, M. A.; Do, H. T.; Miley, G. P.; Silverman, R. B. Inducible nitric oxide synthase: Regulation, structure, and inhibition. *Med. Res. Rev.* **2020**, *40*, 158−189.
(20) Di, L.; Kerns, E. H.; Fan, K.; McConnell, O. J.; Carter, G. T. High throughput artificial membrane permeability assay for blood-brain barrier. *Eur. J. Med. Chem.* **2003**, *38*, 223−232.
(21) Kuzmanic, A.; Zagrovic, B. Determination of ensemble-average pairwise root mean-square deviation from experimental B-factors. *Biophys. J.* **2010**, *98*, 861−871.
(22) Jafari, R.; Almqvist, H.; Axelsson, H.; Ignatushchenko, M.; Lundbäck, T.; Nordlund, P.; Molina, D. M. The cellular thermal shift assay for evaluating drug target interactions in cells. *Nat. Protoc.* **2014**, *9*, 2100−2122.
(23) Jensen, A. J.; Molina, D. M.; Lundbäck, T. CETSA: a target engagement assay with potential to transform drug discovery. *Future Med. Chem.* **2015**, *7*, 975−978.
(24) Olaru, A.; Bala, C.; Jaffrezic-Renault, N.; Aboul-Enein, H. Y. Surface plasmon resonance (SPR) biosensors in pharmaceutical analysis. *Crit. Rev. Anal. Chem.* **2015**, *45*, 97−105.
(25) Wang, S.; Dong, Y.; Liang, X. Development of a SPR aptasensor containing oriented aptamer for direct capture and detection of tetracycline in multiple honey samples. *Biosens. Bioelectron.* **2018**, *109*, 1−7.
(26) Hou, L.; Zhou, X.; Zhang, C.; Wang, K.; Liu, X.; Che, Y.; Sun, F.; Li, H.; Wang, Q.; Zhang, D.; Hong, J.-S. NADPH oxidase-derived H_2O_2 mediates the regulatory effects of microglia on astrogliosis in experimental models of Parkinson's disease. *Redox Biol.* **2017**, *12*, 162−170.
(27) He, X. J.; Nakayama, H. Neurogenesis in Neurotoxin-induced Animal Models for Parkinson's Disease-A Review of the Current Status. *J. Toxicol. Pathol.* **2009**, *22*, 101−108.
(28) Cui, X.; Li, M. P.; He, Z. C.; Hu, L.; Liu, J. P.; Yan, J. H.; Hua, L. M. MiR-302b-5p enhances the neuroprotective effect of IGF-1 in methyl-4-phenyl-1,2,3,6-tetrahydropyridine-induced Parkinson's disease by regulating inducible nitric-oxide synthase. *Cell Biochem. Funct.* **2020**, *38*, 1023−1035.
(29) Alvarez-Fischer, D.; Noelker, C.; Grünewald, A.; Vulinović, F.; Guerreiro, S.; Fuchs, J.; Lu, L.; Lombès, A.; Hirsch, E. C.; Oertel, W. H.; Michel, P. P.; Hartmann, A. Probenecid potentiates MPTP/MPP + toxicity by interference with cellular energy metabolism. *J. Neurochem.* **2013**, *127*, 782−792.
(30) Meka, D. P.; Müller-Rischart, A. K.; Nidadavolu, P.; Mohammadi, B.; Motori, E.; Ponna, S. K.; Aboutalebi, H.; Bassal, M.; Annamneedi, A.; Finckh, B.; Miesbauer, M.; Rotermund, N.; Lohr, C.; Tatzelt, J.; Winklhofer, K. F.; Kramer, E. R. Parkin cooperates with GDNF/RET signaling to prevent dopaminergic neuron degeneration. *J. Clin. Invest.* **2015**, *125*, 1873−1885.
(31) Fan, D.-s.; Ogawa, M.; Ikeguchi, K.; Fujimoto, K.-i.; Urabe, M.; Kume, A.; Nishizawa, M.; Matsushita, N.; Kiuchi, K.; Ichinose, H.; Nagatsu, T.; Kurtzman, G. J.; Nakano, I.; Ozawa, K. Prevention of dopaminergic neuron death by adeno-associated virus vector-mediated GDNF gene transfer in rat mesencephalic cells in vitro. *Neurosci. Lett.* **1998**, *248*, 61−64.
(32) Hevel, J. M.; Marletta, M. A. Nitric-Oxide Synthase Assays. *Methods Enzymol.* **1994**, *233*, 250−258.
(33) Bourdonnec, B. L.; Leister, L. K.; Ajello, C. A.; Cassel, J. A.; Seida, P. R.; O'Hare, H.; Gu, M.; Chu, G.-H.; Tuthill, P. A.; DeHaven, R. N.; Dolle, R. E. Discovery of a series of aminopiperidines as novel iNOS inhibitors. *Bioorg. Med. Chem. Lett.* **2008**, *18*, 336−343.
(34) Do, H. T.; Li, H.; Chreifi, G.; Poulos, T. L.; Silverman, R. B. Optimization of blood-brain barrier permeability with potent and selective human neuronal nitric oxide synthase inhibitors having a 2-Aminopyridine scaffold. *J. Med. Chem.* **2019**, *62*, 2690−2707.
(35) Hu, X.; Song, Q.; Li, X.; Li, D.; Zhang, Q.; Meng, W.; Zhao, Q. Neuroprotective effects of Kukoamine A on neurotoxin-induced Parkinson's model through apoptosis inhibition and autophagy enhancement. *Neuropharmacology* **2017**, *117*, 352−363.
(36) Capitelli, C.; Sereniki, A.; Lima, M. M. S.; Reksidler, A. B.; Tufik, S.; Vital, M. A. B. F. Melatonin attenuates tyrosine hydroxylase loss and hypolocomotion in MPTP-lesioned rats. *Eur. J. Pharmacol.* **2008**, *594*, 101−108.

https://doi.org/10.1021/acs.jmedchem.1c00578
J. Med. Chem. 2021, 64, 7760−7777